ABX_3 perovskites for tandem solar cells

Miguel Anaya,[1] Gabriel Lozano, [1] Mauricio E. Calvo[1] and Hernán Míguez[1*]

[1] Institute of Materials Science of Seville, Spanish National Research Council-University of Seville, Calle Américo Vespucio 49, 41092, Seville, Spain.

[*] h.miguez@csic.es

Summary

Perovskite solar cells carry the banner for emerging photovoltaics since they have demonstrated power conversion efficiency values well above 20%, which were traditionally only accessible for fairly stablished technologies such as silicon. Indeed, ABX_3 perovskite materials have revolutionized solar cells due to its ease of processing and outstanding electronic and optical properties, which make them ideal candidates to develop multi-junction devices aiming to surpass limits associated to standalone technologies. In this review we will discuss late efforts on this matter. First, we introduce the reader standard materials and processing techniques involved in the preparation of state-of-the-art perovskite solar cells. Then, we discuss the development of perovskite-based tandem devices in which ABX_3 perovskite acts as the active material in the top subcell and Si, CIGS, polymer or ABX_3 as bottom subcells. Finally, we provide the reader with a discussion on the different lines of research that this rapidly developing field may follow.

Introduction

In a world where the energy demand is still governed for more than 80% by fossil fuels, any realistic path reach the objective of reducing CO_2 emissions and prevent a further increase of the global average temperature must have renewable energy as its core. [1,2] In this scenario, solar energy surpasses by orders of magnitude the potential of all the other renewable alternatives combined, as it is displayed in Figure 1a.[3] Consequently, solar photovoltaic technologies (PV) are attracting tremendous social interest: markets are rapidly increasing their investments on PV, and academia is devoting tireless efforts to study the mechanisms of solar to electrical energy conversion in order to push efficiency limits. Figure 1b displays the evolution of the number of scientific articles related to PV published since 1980, which reflects a continuously growing interest towards the development of solar technologies.[4] In this context, solar cells

based on metal halide (ABX_3) perovskites emerged in the last decade as a new technology that demonstrates both high performance and low cost. This type of cells are driving a revolution in PV, holding great promise for the generation of green energy at large scale. Indeed, perovskite solar cells (PSCs) represent already a 10% of all papers published in the field of PV and they have been recently highlighted as one of the top ten emerging technologies according to the World Economic Forum.[5] This is due to the natural abundance of the precursors employed to synthesize perovskite absorbers, their weightlessness and, above all reasons, the swift rise in power conversion efficiency (PCE) demonstrated for this technology. All these facts make perovskite devices potential competitors of well stablished technologies such as those based on silicon. Not in vain PSCs evolved from featuring a modest 3.81% in 2009[6] to over 20% in several works nowadays,[7] which reveals PSCs as the most efficient emerging PV devices.[8,9] Along with the efficiency, scientists are intensively working to develop perovskite materials and PSCs that are environmental friendly and stable over time.

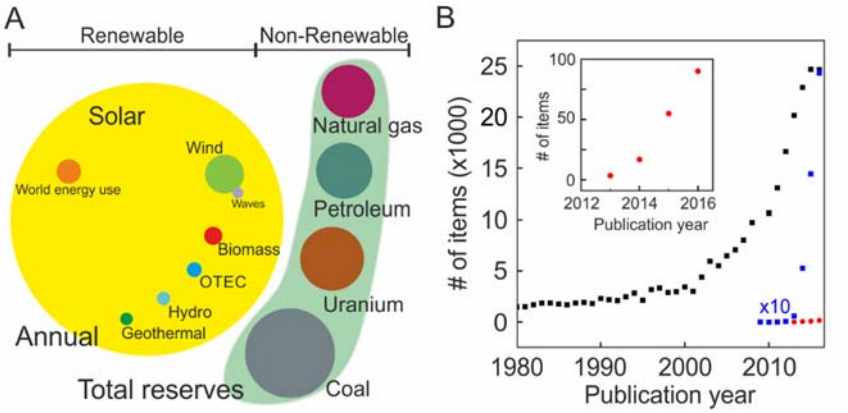

Figure 1. (a) Comparative of finite and renewable planetary energy reserves in 2015. Total recoverable reserves are shown for the finite resources. Yearly potential is shown for the renewables (Reproduced with permission from reference 3). (b) Results of the searchs 'photovoltaic and solar cell', "perovskite solar cell" and "perovskite tandem solar cell" in the Web of Science.

Photo-conversion record efficiencies of PSCs are approaching the thermodynamic limit established by the Shockley-Queisser (SQ) theory, which sets the maximum PCE achievable for single junction cells depending on the bandgap energy (E_{bg}) of the absorbing material.[10] Different strategies can be employed to surpass such theoretical ceiling but only a few have been studied for perovskite devices. Hot-carriers have been demonstrated to travel up to 600 nm in $CH_3NH_3PbI_3$ ($MAPbI_3$) perovskite films but, in order to take advantage of this phenomenon, it will be necessary to develop energy-selective contacts.[11,12] Also, recent simulations suggest that multi-exciton generation might be possible in perovskites that show quantum confinement, but experimental demonstration remains a big challenge.[13] Although such

approaches may open new avenues for the development of devices that take advantage of photon energy excess to surpass SQ limits, their demonstration in actual devices seems difficult. On the other hand, multi-junction or tandem configurations have already proven to improve PCEs over the limits imposed by SQ theory. The working principle of tandem solar cells is based on the combination of different subcells, each of them able to absorb a different part of the electromagnetic spectrum, which allows minimizing losses and reaching higher PCEs. In a standard single-junction solar cell, photons with energies lower than the E_{bg} of the active material cannot be absorbed while those with higher energies lead to carriers that eventually thermalize to band edges from where they are extracted. These undesirable effects result in current and potential losses, respectively. In contrast, a double-junction configuration combines top (front) and bottom (rear) subcells based on materials with absorption onsets at relative shorter and longer wavelengths (see Figure 2a). In Figure 2b we present canonical energy diagrams for a double-junction tandem cell. Photons with higher energies are harvested in the front cell while those of lower energies penetrate deeper in the device and are absorbed by the rear cell. As it happens for single junction devices, it exists a thermodynamic limit imposed by the SQ theory also in the case of double junction (tandem) solar cells. That leads to an optimal combination of E_{bg} for the front and rear cells.

It is possible to classify double junction cells as two- or four-terminal devices based on the electric connection among subcell electrodes. In a two-terminal device, subcells are monolithically stacked requiring a recombination layer or a tunnel junction in order to achieve charge neutrality (see Figure 2c). In this series connection scheme, currents through top and bottom cells must be the same, being thus limited by the subcell that produces a lower photocurrent. A four-terminal tandem solar cell is composed by two self-working cells that are externally connected in series or in parallel as convenience. As displayed in Figures 2d and 2e, they can be either mechanically stacked or coupled by optical filters. From a fabrication point of view, four-terminal devices are more convenient since the preparation techniques of the different junctions do not need to be compatible. Nevertheless, two terminal configurations are more attractive from an industrial point of view since they present lower parasitic absorption and costs are reduced due to the less amount of transparent conductive material required.

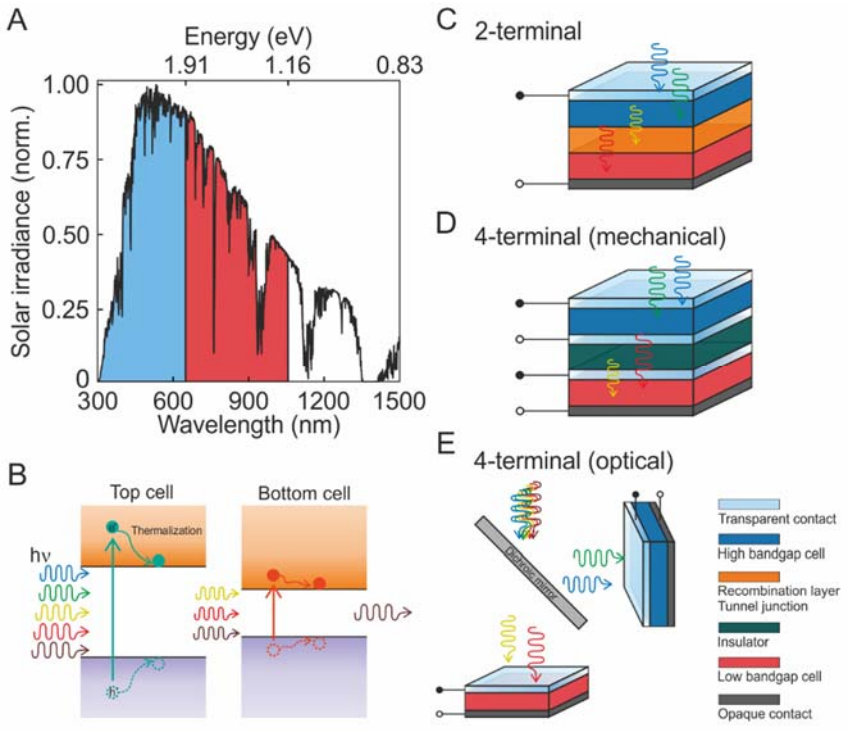

Figure 2. (a) Spectral response of generic top (blue) and bottom (red) subcells comprising a tandem device working in different regions of the reference solar spectral irradiance AM1.5. (b) Canonical energy diagram for a double-junction tandem solar cell. Scheme of the three most common double-junction configurations: (c) two terminal, (d) mechanically stacked four terminal, and (e) optically coupled four terminal.

Tandem architectures have been widely employed in several PV technologies such as Si, III-V semiconductor or organic solar cells in order to boost their performance.[14,15,16] In fact, the most efficient PV device ever fabricated is based on expensive multi-junction configurations based on different semiconductors,[8] whose primarily application is related to self-powered systems installed in the outer space.[17] In this context, ABX_3 perovskite materials, which are easy to process and feature a tuneable bandgap, offer a cost effective alternative for producing highly efficient tandem solar cells. Thus interest for this option is growing in the last years (see inset of Figure 1b).

Herein, we present a review on the use of ABX_3 perovskites for tandem solar cell applications. Firstly, we introduce this family of materials, paying special attention to their fabrication methods and optoelectronic properties. Then, we discuss perovskite-based single junction solar cells in the context of SQ limit. Afterwards, we provide a thorough revision on the different demonstrations of perovskite-based tandem devices. PSCs can be combined as front subcells with well-stablished technologies that operate as rear subcells such as silicon, copper indium gallium selenide (CIGS) or organic PV devices., reaching outstanding efficiencies. Also, perovskite materials with different E_{bg} can be combined in tandem solar cells. In fact, we show that all-perovskite tandem devices represent a unique opportunity to develop third-

generation PV for widespread use. We finish with an outlook in which we share our view on the paths the community may follow in order to push the efficiency of ABX_3 perovskite based tandems towards new horizons.

ABX_3 perovskite materials for single junction solar cells

In the most simplified description, ABX_3 perovskites consist on a hexa-coordinated metal (B) cation occupying the centres of octahedra which share their halide-type (X) corners; a cation (A) fills the voids left by every eight of those octahedra (see Figure 3a), located at the corners of a classical cubic cell. Among perovskite materials developed for PV, methyl-ammonium lead triiodide ($MAPbI_3$) is the most widely employed compound. It presents a tetragonal structure (space group *I4cm*) at room temperature with two phase transitions: one at 160 K to an orthorhombic structure (space group *Pnma*), and another one at 327 K to cubic.[18,19,20] At operational conditions, its absorption onset is placed at λ=780 nm (E=1.6 eV) and its absorption coefficient is high enough to absorb 100% of the photons provided by the sun with energies higher than the bandgap with only 1 μm of material.[21] Resulting excitons perform as low as 6 meV binding energy at room temperature, which allow them to be separated in free electrons and holes very quickly.[22] Also, these carriers feature diffusion lengths in the order of microns, which lead to efficient charge extraction.[23] From a complementary point of view, perovskite materials show high radiative recombination rates that make them very interesting for light emission applications.[24,25,26,27]

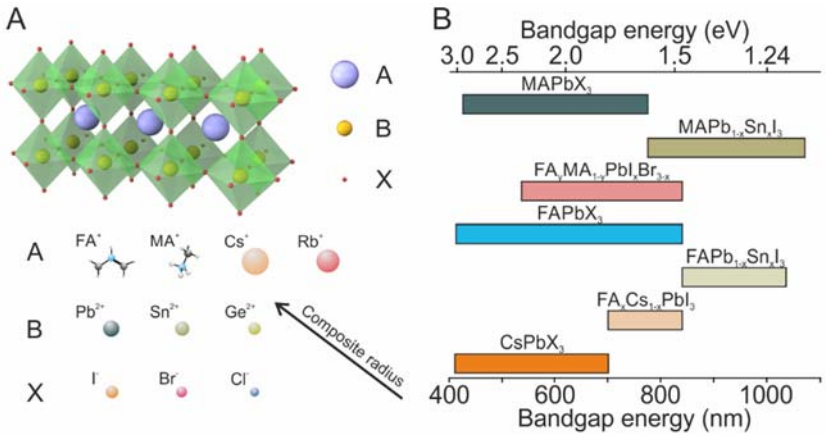

Figure 3. (a) Schematic illustration of an ABX_3 perovskite and typical elements occupying the different positions in the structure. (b) Bandgap energies that can be attained with the different combinations of elements in an ABX_3 perovskite structure.[28,29,30,31,32,33,34,35,36]

Processing

ABX_3 perovskite films are integrated as active layers in solar cells using spin coating,[37,38,39,40]dip coating,[41] spray coating,[42] thermal co-evaporation,[43,44] chemical vapour deposition,[45] and vapour phase conversion,[46] among others. Solution processing methods amenable for mass production can be employed due to the large tolerance perovskites feature against structural defects in contrast to most semiconductors.[47] These techniques enable the integration of perovskite films in tandem devices since they are compatible with the processing of other PV technologies. Among all preparation methods reported, spin coating dominates the scenario, being the anti-solvent approach the one leading to better film quality and reproducibility.[39,40]

Bandgap tunability

One of the biggest advantages ABX_3 perovskites offer with respect to other semiconductor materials is the possibility to tune their absorption onset *a la carte* by ion replacement, while involving easy and cost-effective solution process methods. A, B, and X sites present in the $MAPbI_3$ crystal can be successfully substituted, leading to optical absorption edges easily tuneable within the 350 to 1200 nm wavelength range, as shown in Figure 3b.

X-site substitution. The most common modification in the formulation of perovskites is based on halide replacement. The breakthrough in this regard was presented by Seok et al.[28] who demonstrate iodine replacement by bromine in $MAPbI_3$. This opened the path for chemical management in perovskites. Nowadays it is possible to find in the literature both $MAPbBr_xI_{3-x}$ and $MAPbCl_xBr_{3-x}$ perovskite films with bandgaps covering the entire visible spectrum. As the biggest halide, I^-, is substituted by a smaller one, being $I^- > Br^- > Cl^-$, the absorption onset is gradually blue-shifted. In particular, the electronic bandgap of the $MAPbX_3$ family can be shifted from E_{bg}=1.6 eV ($MAPbI_3$) to as far as E_{bg}=2.3 eV ($MAPbBr_3$), and from E_{bg}=2.3eV ($MAPbBr_3$) to as far as E_{bg}=3.1eV ($MAPbCl_3$)..[29]

B-site substitution. In the search of Pb-free perovskites, the Pb^{2+} cation, which occupies the B site in the perovskite structure, has been substituted by Ge^{2+},[48] and Sn^{2+}.[19] The latter has been studied more intensively as it provides the most feasible way to attain perovskite materials that absorb in the near infrared, up to 1.17 eV.[30,49,50,51]

A-site substitution. The MA^+ cation has been also substituted by formamidinium ($CH(NH_2)_2^+$, abbrev. FA^+) or Cs^+ ion. FA^+ is the preferred candidate to substitute the organic cation.[32] The deep electronic states associated to either MA^+ or FA^+ should imply a slight modification of the bandgap upon

substitution.[52] Nevertheless, the larger size of FA^+ tilts the metal-halide octahedra decreasing the bandgap from 1.6 eV for $MAPbI_3$ to 1.45 eV for $FAPbI_3$.[34,53]Also, Cs^+ cations have been succesfully employed in the preparation of full inorganic Pb- or Sn-based perovskites that feature E_{bg} shifted to shorter wavelengths.[54,55] These approaches may be combined with Br^- substitution to further blue-shift the bandgap of the FA or Cs-based perovskites.[32,56,57]

The substitution of the A site combined with mixtures of halides or metals has been reported, namely, $FA_yMA_{1-y}PbI_xBr_{3-x}$,[31,58]$FA_yCs_{1-y}$ PbI_xBr_{3-x},[59,60]and $FA_yCs_{1-y}PbSnI_3$.[34,50] It is claimed the use of Cs^+ mitigates halide segregation or Sn^{2+} oxidation. Similarly, the use of triple Cs/MA/FA and even quadruple Rb/Cs/MA/FA cation based perovskites has been proven to yield devices with improved stability.[61,62] In particular, the incorporation of Rb to the perovskite composition enhances its durability under moisture.[63]

Single-junction devices

As we mentioned before, electro-optical properties, ease of processing and versatility are the factors that explain the irruption of ABX_3 perovskites for PV applications. Figure 4a shows a scheme of the typical solar cell. The device is composed by a glass substrate covered with a transparent conductive electrode, usually fluorine doped tin oxide (FTO) or indium tin oxide (ITO). Then, an electron selective layer (ESL), a perovskite film and a hole selective layer (HSL) are sequentially deposited. Finally, a thermally evaporated metallic film is commonly used as a back contact to electrically close the cell. Perovskite material can be supported by a mesoporous scaffold that can be an electric conductor as TiO_2[38] or an insulator as Al_2O_3.[37] A selection of conventional materials employed in the fabrication of perovskite solar cells is presented in Figure 4a. If a scaffold is employed we refer to the cell as mesostructured, otherwise it is named planar. Albeit the described architecture is the dominant and therefore considered as standard in the perovskite community, there are examples in which the relative position of the ESL and HSL with respect to the perovskite layer are interchanged. This latter architecture is called inverted.[64]

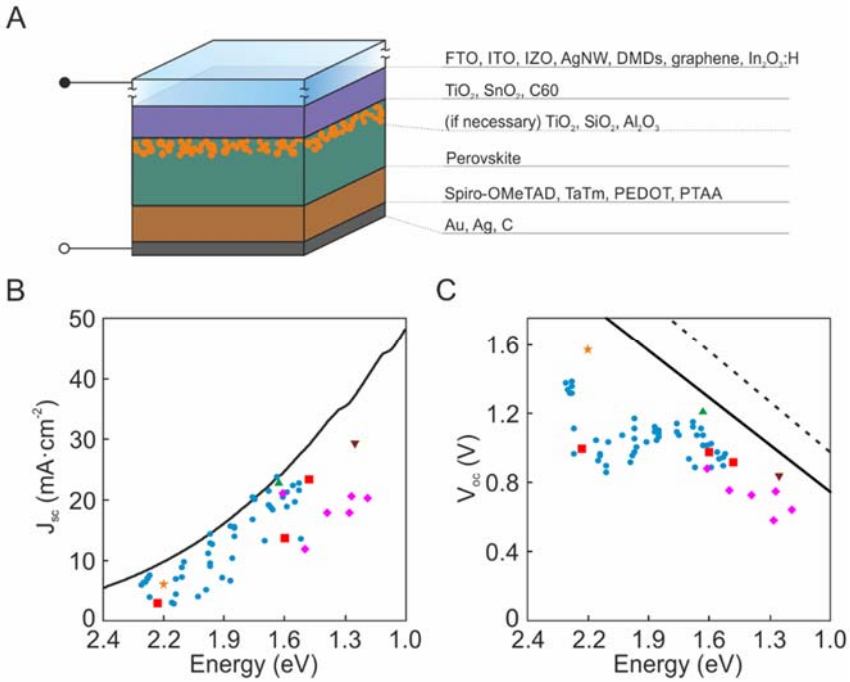

Figure 4. (a) Scheme of the standard architecture of a perovskite solar cell and a catalogue of materials employed for the preparation of the different layers comprising the device. Calculated ideal short circuit current (b) and open circuit voltage (c) as a function of the bandgap energy of the absorber material according to Shockley-Queisser theory. A selection of the best experimental parameters found in the literature is also plotted: ref. 31 (blue circles), ref. 32 (red squares), ref. 65 (yellow star), ref. 62 (green triangle), ref. 66 (pink diamonds), and ref. 67 (brown triangle).

Here, we will focus exclusively on the main performance parameters of state-of-the-art devices. Figures 4b and 4c displays the classical PV parameters obtained by solving the SQ equation for an ideal device based on a E_g bandgap material operating at 300 K.[10] A selection of the best experimental parameters found in the literature as a function of the E_{bg} of the ABX_3 perovskite material, regardless of its composition, are also plotted in Figures 4b and 4c.[31,32,62,65,66] It can be observed that, generally, J_{sc} and V_{oc} are close to the thermodynamic limit. In particular, the highest J_{sc} reported for a 1.6 eV bandgap perovskite reaches a value of 23 mA/cm^2,[68] which is the maximum achievable value when optical losses are considered. In addition, a V_{oc} of 1.24 V is attained for a bandgap of 1.63 eV,[62] which represents a 0.39 V loss, the second smallest difference value measured for any PV technology.[69]

Perovskite based double junction solar cells

Tandem devices bear the promise of an even better photovoltaic performance than that achieved with single junction ones. Perovskites have been widely employed for the experimental demonstration of tandem devices as it is summarized in tables 1, 2, and 3. In general, ABX_3 materials have been proposed as top subcell light harvesters combined with bottom subcells based on Si, CIGS and other stablished technologies. More recently, the possibility of attaining narrow bandgap perovskites has inspired the

fabrication of all-perovskite tandem solar cells. Main results reported in the literature are discussed in what follows. We will focus on how the use of different materials, the way these are processed or integrated into an operating solar cell impact the power conversion efficiency of the operating device. It is worth to mention that measuring efficiencies from J-V curves multi-junction is very delicate because of the spectrum mismatch of commercial solar simulators. To overcome this issue, in general, spectrally adjustable solar simulators are required, in which the extracted photocurrent is calibrated to match that calculated by external quantum efficiency (EQE) measurements of reference subcells.[70] Thus, relative EQE spectra must be accurately taken by illuminating the corresponding reference subcell with chopped monochromatic light, and using spectrally filtered constant-light bias to turn on the reference subcell that is not being measured. Indeed, devices with voltage-dependent quantum efficiency (i.e. amorphous silicon) require applying a voltage bias. In addition to efficiency, other parameters such as the life cycle or the manufacturing costs must be considered when assessing the technological impact of perovskite-based tandem devices. In particular, cost calculations take into account component, architecture and fabrication methodology of the solar module. However, the greatest uncertainty when elaborating cost models originates from the evolution of the power conversion efficiency of the cell over the next years.[71]

Perovskite/Si

The combination of perovskite and silicon solar cells in tandem configurations is of great interest due to the possibility of boosting efficiencies above 30% while reducing the cost per kilowatt. Silicon has experienced a massive industrial scaling process in the last decades and nowadays represents the dominant technology in the PV market with the advent of commercial solar modules that reach around 16% average efficiency. Moreover, the 26.6% record efficiency that can be obtained in laboratory prototypes is very close to the 29.1% theoretical ceiling predicted for a 1.1 eV bandgap material.[8,72]

Two-terminal Si-based devices. Mailoa et al. presented in March 2015 the first demonstration of a two-terminal perovskite/Si tandem solar cell (see Figure 5a).[73] They fabricated a standard mesoporous $MAPbI_3$ based subcell with silver nanowires (AgNWs), Spiro-OMeTAD and TiO_2 acting as front contact, HSL and ESL, respectively, on top of an n-type Si subcell. In order to allow the recombination of electrons from perovskite passing through the TiO_2 film with holes arising from the Si-based subcell, an n^{++}/p^{++} tunnel junction was utilised. This layer consists on a heavily doped n^{++} hydrogenated amorphous silicon (a-Si:H) deposited via plasma-enhanced chemical vapour deposition combined with a p^{++} Si

emitter. The device performs a moderate 13.7% with a significant hysteresis, which is probably due to the use of not state-of-the-art perovskite and silicon materials (Figure 5b).

In order to fabricate double-junction devices based on the best performing silicon technology, i.e. the a-Si:H/c-Si silicon heterojunction (SHJ), it is needed to work at temperatures below 200 ºC to prevent undesirable H mobility at the a-Si:H layer. With this in mind, Albretch et al. reported a low-temperature approach for the complete fabrication process of the tandem device.[74] They replaced the standard TiO_2 ESL, which requires a ~500 ºC annealing, by a SnO_2 ESL deposited at room temperature by atomic layer deposition (ALD). In this case, the recombination layer between subcells is formed by SnO_2 and ITO film. Moreover, better quality perovskite composition, $FA_yMA_{1-y}PbI_xBr_{3-x}$, and a Spiro-OMeTAD/$MoO_3$/ITO front contact were used to prepare the top cell. The combination of those improvements pushes the perovskite/silicon tandem solar cell performance to stabilised power conversion efficiency (PCE) of 18.1%. In addition, Werner et al. showed that low-temperature organic PEIE/PCBM ESL could be used to substitute the standard TiO_2 ESL in order to attain devices with a recombination layer based on indium zinc oxide (IZO) between perovskite and SHJ subcells.[75] Furthermore, devices yield high currents thank to the subsequent deposition of MoO_x, IO:H (hydrogenated In_2O_3) and ITO as transparent front contact resulting in a hysteresis-free 19.2% efficiency device of 1.22 cm^2.

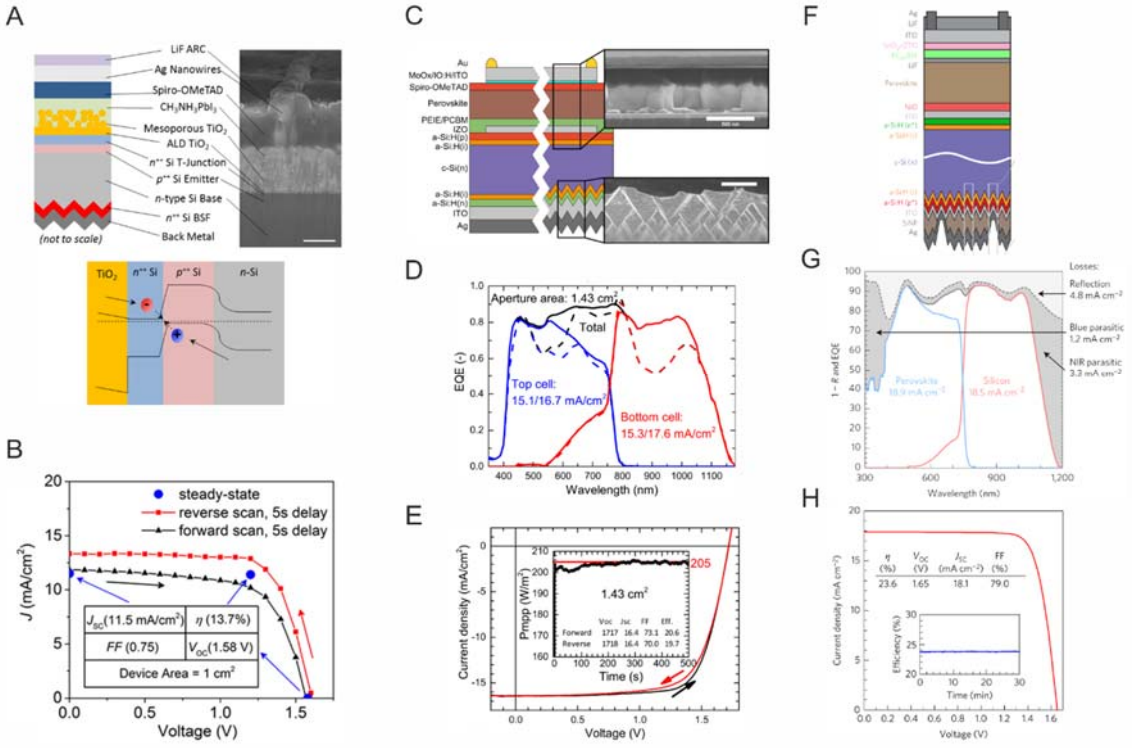

Figure 5. Two terminal perovskite/silicon tandem solar cells structure and band diagram (a) and J-V curve (b) of a device where a tunnel junction is employed as intermediate layer. Reprinted from reference 73, with the permission of AIP Publishing. Structure (c), EQE spectra (d) and J-V curve (e) of a 1.43 cm^2 device with IZO as recombination layer. Solid and dashed lines in the EQE spectra correspond to the same solar cell measured with and without antireflective layer, respectively (Reproduced with permission from reference 76). Structure (f), EQE spectra (g) and J-V curve (h) of the record monolithic perovskite/silicon tandem device. Adapted by permission from Macmillan Publishers Ltd: Nature Energy (77), copyright 2017.

As pointed out by the exhaustive work of Filipic and others, [78,79,80,81,82,83] the use of randomly distributed pyramids to texture the c-Si surface reduces the reflection and increases the optical path length in the cell. Indeed, as shown in Figure 5c, Werner et al. make use of this effect to increase the efficiency of a 1.43 cm^2 two-terminal perovskite/silicon tandem device from 19.2%[73] to 20.5% (Figures 5d and 5e).[76] Nevertheless, concerns over the long stability of this tandem configuration rise since the MoO_x HSL may react with the perovskite.[84]

More recently, the experimental demonstration of a more stable perovskite, with $Cs_{0.17}FA_{0.83}Pb(Br_{0.17}I_{0.83})_3$ formulation,[60] has opened the path to a record perovskite/silicon double-junction device, developed by Bush et al.[77] They made a perovskite solar cell in which the thermal and moisture stability of the perovskite compound tolerates the sequential deposition of SnO_2, ZTO and ITO by ALD, pulsed-chemical vapor deposition and sputtering, respectively, as electron selective front contact of the solar cell. This transparent contact window ensures negligible parasitic absorption and acts as diffusion barrier, leading to 23.6% efficiency as displayed in Figures 5f-h.

Type	Device architecture Top cell Bottom cell	J_{sc} ($mA \cdot cm^{-2}$)	V_{oc} (V)	FF	Efficiency (%)	Size (cm^2)	Reference (year)
2T	LiF/AGNWs/Spiro/mpTiO_2-$MAPbI_3$/TiO_2 a-Si:H/a-Si/p^{++} Si/n-Si/n^{++} Si/metal	11,5	1,58	0,75	13,7	1,00	73 (2015)
2T	LiF/ITO/MoO_3/Spiro/FAMAPbIBr/SnO_2/ITO a-Si:H(p^+)/a-Si:H(i)/c-Si/a-Si:H(i)/a-Si:H(n^+)/AZO/Ag	12,9	1,78	0,79	18,1	0,16	74 (2015)
2T	ITO/IO:H/MoO_x/Spiro/$MAPbI_3$/PCBM/PEIE/IZO a-Si:H(p^+)/a-Si:H(i)/c-Si(n)/a-Si:H(i)/a-Si:H(n^+)/ITO/Ag	16.1 (15.9)	1.701 (1.690)	0.701 (0.776)	19.2 (21.2)	1.22 (0.17)	75 (2015)
2T	ITO/IO:H/MoO_x/Spiro/$MAPbI_3$/PCBM/PEIE/IZO a-Si:H(p^+)/a-Si:H(i)/c-Si(n)/a-Si:H(i)/a-Si:H(n^+)/ITO/Ag	16,4	1,717	0,731	20,5	1,43	76 (2016)
2T	**LiF/ITO/SnO_2-ZTO/PCBM/LiF/$FA_{0.83}Cs_{0.17}PbI_{2.49}Br_{0.51}$/NiO/ITO a-Si:H($n^+$)/a-Si:H(i)/c-Si(n)/a-Si:H(i)/a-Si:H(p^+)/ITO/SiNP/Ag**	**18,10**	**1,65**	**0,79**	**23,6**	**1,00**	**77 (2017)**
4T	LiF/FTO/TiO_2/mpTiO_2-$MAPbI_3$/Spiro/AgNWs/LiF SiN_x/emitter/mc-Si/Al	17.5 11.1	1.025 0.547	0.710 0.704	12.7 4.3	0.39 0.39	85 (2014)
4T	FTO/TiO_2/mpTiO_2-$MAPbI_3$/Spiro/MoO_x/ITO ITO/a-Si:H(p+)/a-Si:H(i)/c-Si(n)/ITO/Ag	14.5 13.7	0.821 0.689	0.519 0.767	6.2 7.2	0.25 4.00	86 (2014)
4T	MgF_2/ITO/TiO_2/mpTiO_2-$MAPbI_3$/Spiro/MoO_x/ITO/MgF_2 PERL silicon solar cell	18.8 16.9	0.950 0.640	0.690 0.730	12.2 7.9	0.25 4.00	87 (2016)
4T	FTO/TiO_2/mpTiO_2-$MAPbI_3$/Spiro/MoOx/IZO a-Si:H/c-Si(n)	17.5 14.6	0.870 0.690	0.680 0.776	10.36 7.82	0.16 4.00	88 (2015)
4T	FTO/TiO_2/mpTiO_2-$MAPbI_3$/Spiro/MoOx/IZO a-Si:H/c-Si(n)	19.0 17.0	1.090 0.720	0.647 0.767	13.4 9.40	0.16 4.00	89 (2015)
4T	ITO/IO:H/MoO_x/Spiro/$MAPbI_3$/PCBM/PEIE/IZO ITO/a-Si:H(p^+)/a-Si:H(i)/c-Si(n)/a-Si:H(i)/a-Si:H(n^+)/ITO/Ag	19.3 (20.1) 15.5 (16.0)	1.057 (1.070) 0.692 (0.693)	0.710 (03755) 0.794 (0.795)	14.4 (16.2) 8.5 (8.8)	1.00 (0.25) 1.00 (0.25)	76 (2016)
4T	MgF_2/ITO/PEDOT:PSS/$MAPbI_3$/PCBM/AZO/ITO/MgF_2 c-Si cell	16.5 13.3	0.952 0.562	0.774 0.762	12.3 5.7	0.39 0.39	90 (2016)
4T	ITO/PTAA/$MAPbI_3$/PCBM/C60/BCP/Cu/Au/BCP IZO/a-Si:H(p+)/a-Si:H(i)/c-Si(n)/a-Si:H(i)/a-Si:H(n+)/ITO/MgF_2/Ag	20.6 12.3	1.080 0.679	0.741 0.779	16.5 6.5	0.08 4.00	91 (2016)
4T	FTO/SnO_2-PCBM/$FA_{0.83}Cs_{0.17}PbI_{1.8}Br_{1.2}$/Spiro/ITO ITO/a-Si:H(p+)/a-Si:H(i)/c-Si(n)/a-Si:H(i)/a-Si:H(n+)/AZO/Ag	19.9 13.9	1.100 0.690	0.707 0.764	15.1 7.3	0.09 4.00	60 (2016)
4T	**ITO/TiO_2/Rb-$FA_{0.75}(MA_{0.6}Cs_{0.4})_{0.25}PbI_2Br$/PTAA/$MoO_x$/ITO/$MgF_2$ SiO_x/SiN_x/c-Si(n)/emitter (p)/SiO_2/Si_3N_4/Al**	**19.4 18.8**	**1.130 0.690**	**0.700 0.800**	**16.0 10.4**	**0.16 4.00**	**92 (2017)**
4T (opt)	**FTO/TiO_2/mpTiO_2-$MAPbI_3$/Spiro/Au MgF_2/TCO/a-Si:H(p+)/a-Si:H(i)/c-Si(n)/a-Si:H(i)/a-Si:H(n+)/TCO/Ag**	**10.6 34.9**	**0.987 0.728**	**0.715 0.809**	**7.5 20.5**	**0.20 4.00**	**93 (2015)**
4T (opt)	FTO/TiO_2/mpTiO_2-$MAPbBr_3$/Spiro/Au PERL silicon solar cell	7.20 31.6	1.265 0.673	0.720 0.800	6.5 16.9	0.05 1.00	94 (2015)

Table 1. Perovskite/silicon tandem devices reported in the literature. Double junction architecture as well as short circuit current (J_{sc}), open circuit voltage (V_{oc}), fill factor (FF), efficiency, and active area of the devices are summarized. 2T, 4T and 4T (opt) refer to two-terminal, mechanically stacked four-terminal and optically coupled four-terminal architectures, respectively. Words highlighted in blue and red correspond to transparent contacts and recombination layers, respectively. Bold rows point out the record devices for each configuration.

Four-terminal Si-based devices First reports on mechanically stacked four-terminal tandem devices based on perovskite/silicon came out in late 2014. Bailie et al. pioneered the field by using as top subcell a standard FTO/TiO_2/perovskite/Spiro-OMeTAD device in which a transparent silver nanowire (AgNW) mesh was employed as back contact.[85] AgNW is mechanically transferred on top of Spiro-OMeTAD without damaging the structure and replacing other commonly employed opaque contacts such Au. This results in a 12.7% efficiency device with a transmittance of 60-77% in the 800 nm to 1200 nm range. When an 11.4% efficiency multicrystalline silicon solar cell is employed as rear device in the tandem

configuration the performance is improved up to a 17% (Figures 6a and 6b). Other approach consists on the use of transparent conductive oxides (TCOs) as back contact in the perovskite solar cell. In this regard, Löper and co-workers employed a MoO_x buffer layer to deposit an ITO transparent contact to attain a 13.4% efficiency four-terminal perovskite/c-silicon tandem device.[86] Afterwards, Duong et al. optimized the performance of such a design to reach a 20.1%.[87] In other approach, Werner et al. developed a device with a 22.8% performance when IZO acts as back contact instead of ITO in a perovskite-based top cell placed on top of a a-Si/c-Si device.[88,89] Later, as previously discussed, a textured SHJ as back sub-cell allows boosting the efficiency of a four-terminal device to 25.2% and 23% for 0.25 cm^2 and 1 cm^2 areas, respectively.[76] The eventual chemical reaction between MoO_x and iodide motivates its substitution by Al:ZnO nanoparticles as buffer layer to prevent damage from ITO sputtering. Bush et al. developed this idea to attain 18% mechanically stacked $MAPbI_3$/c-silicon tandems stable at 100 ºC in ambient atmosphere.[90]

Chen et al. further optimised the IR-performance of the a-Si/c-Si device by i) incorporating an antireflective coating based on SiO_x and IZO, and ii) by depositing a patterned MgF_2 layer in order to increase the internal reflection and to prevent the light reaching the lossy Ag reflector. Simultaneously, the IR-transparency of the perovskite device was achieved thanks to a 1 nm Cu/ 6 nm Au/40 nm BCP back contact which allows keeping the high performance. When both cells are combined in a four-terminal architecture, an power conversion efficiency of 23% is achieved.[91]

The use of $MAPbI_3$ in the front subcell arise from its condition of standard material in the field, but its 1.6 eV bandgap is far from the optimum ~1.75 eV bandgap needed when considering Si devices for tandem architectures. McMeekin et al. proposed a 1.74 eV bandgap $FA_{0.83}Cs_{0.17}Pb(I_{0.6}Br_{0.4})_3$ perovskite as photo-active material in a transparent perovskite device employed as filter for a SHJ cell. The complete system has a 22.4% PCE.[60] The same idea has been recently followed by Duong and co-workers to further optimise the formulation of the perovskite.[92] The proved beneficial addition of Rb to the perovskite composition[62] permits obtaining a 1.73 eV bandgap Rb-$FA_{0.75}MA_{0.15}Cs_{0.1}PbI_2Br$ material with an improved stability and a favourable bandgap for its application in a double-junction configuration. As displayed in Figures 6d and 6e, combined with a 23.6% interdigitated back contact silicon cell, this approach leads to the four-terminal perovskite/silicon device with the highest performance reported, 26.4%, and negligible hysteresis.[92]

As we pointed out in a previous section, in contrast to mechanical stacking, optical coupling constitutes an alternative route to achieve four-terminal tandem devices. They are founded on the use of a dichroic mirror which splits sunlight radiation by reflecting short wavelength photons and transmitting long wavelength ones. Uzu et al. reported in early 2015 the first version of this subclass of tandem devices by combining a standard FTO/TiO_2/$MAPbI_3$/Spiro/Au solar cell with a SHJ device (see Figure 6f).[93] The optical splitter reflects photons with $\lambda<550$ nm to the perovskite device, transmitting the remaining photons towards the SHJ device. J-V characteristics of the complete cell are displayed in Figure 6g. A total efficiency of 28% is achieved, which is limited by the 7.5% efficiency of the perovskite solar cell. The use of 1.6 eV bandgap material to harvest 350 nm$<\lambda<$550 nm photons is at the origin of the moderate performance observed, due to the poor voltage attained, which could have been much higher if an optimum 2.25 eV bandgap perovskite had been employed. With this starting point, Sheng and co-workers replaced $MAPbI_3$ by $MAPbBr_3$ perovskite (E_{bg}= 2.3 eV).[94] However, the far-from-ideal 8.8% efficiency of the standalone $MAPbBr_3$ device also mitigates the efficiency of a tandem architecture: while a passivated emitter with rear locally diffused (PERL) Si cell presents a 22.7% efficiency, the optically coupled device shows just a slightly higher 23.4%. Moreover, the authors proposed for the first and only time a full perovskite tandem device where a $MAPbBr_3$- and a $MAPbI_3$- based devices are optically coupled to reach a 13.4% efficiency. The approach discussed in this paragraph presents serious concerns in terms of an eventual industrial viability since the required optical filters are costly. Kinoshita et al. showed a tandem cell in which a dye-sensitized solar cell (DSSC) is employed instead of a silicon one.[95] The DSSC is based on the DX3 dye capable of harvesting photons up to 1100 nm, similarly to silicon, resulting in a remarkable J_{sc}=30.3 mA/cm^2 when the full solar spectrum illuminates the DSSC. Nevertheless, its overall PCE is 10.2% due to a modest V_{oc}=0.556 V. This fact hampers the total performance of the optically coupled four-terminal perovskite/dye tandem device to 21.5%, compared to the 28% obtained from a SHJ.[93]

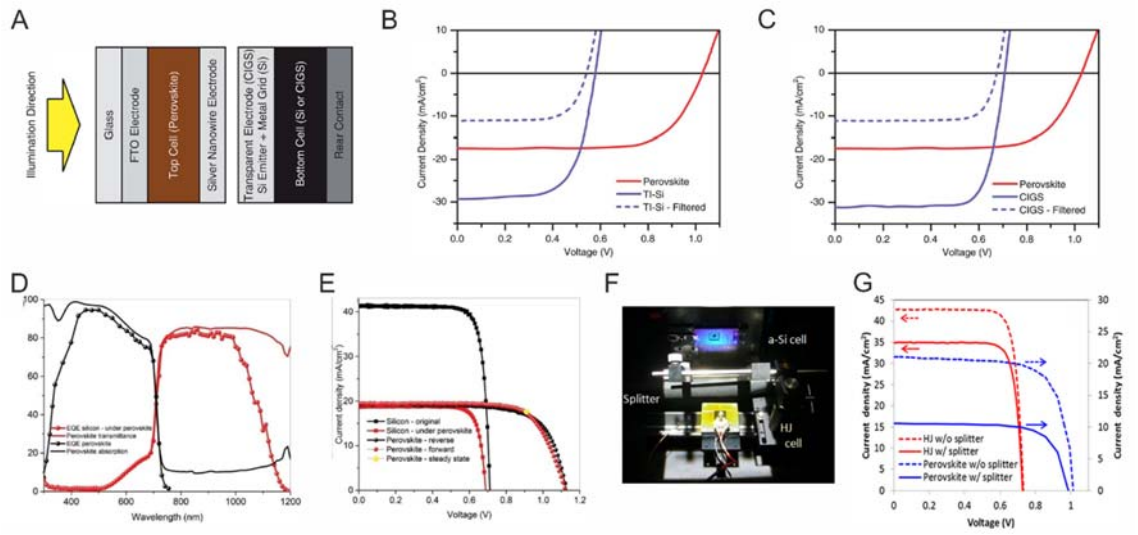

Figure 6. Four-terminal perovskite/silicon tandem solar cells Structure (a) and J-V curves of a perovskite/silicon (b) and perovskite/CIGS (c) tandem solar cell where silver nanowires are employed as transparent rear contact in the perovskite based top subcell. Adapted from Reference 85 with permission of the Royal Society of Chemistry. EQE spectra (d) and J-V curve (e) of the record mechanically stacked four-terminal perovskite/silicon tandem device. Adapted with permission of John Wiley & Sons Ltd from Reference 92. Measurement setup (f) and J-V curve (g) of an optical splitting system. Reprinted from Reference 93, with the permission of AIP Publishing.

Perovskite/Chalcogenide

CIGS solar cells are considered realistic candidates for substituting silicon devices in the PV industry. The high extinction coefficient of this semiconductor allows absorbing light very efficiently with films of just a few microns, much thinner than typical Si films employed in Si solar cells. Moreover, CIGS can be developed in flexible substrates and thus incorporated to roll-to-roll based production chains which are of special interest from an economic point of view. Nowadays, the record CIGS solar cell presents an efficiency of 22.6%.[8,9] In order to drive that value forward, the combination of CIGS cells with perovskite materials in tandem configuration has also been explored. The possibility to tune the bandgap of CIGS materials from 1.1 to 1.24 eV and perovskite from 1.17 eV to 3.1 eV pave the way to the realization of tandem solar cells in which both front and rear cells present an optimized bandgap. In order to integrate both technologies it is essential to maintain the whole fabrication process below 200 ºC, as the p-n junction in CIGS degrades at higher temperatures.

Two-terminal CIGS-based devices. Todorov et al. proposed the first two-terminal perovskite/CIGS tandem solar cell in September 2015.[96] They employed a 1.04 eV bandgap CIGS absorber to fabricate the back subcell with a CdS/CIGS/Mo/Si_3N_4/glass configuration. It should be noticed that the intrinsic ZnO layer commonly employed in CIGS devices is supressed as it degrades the perovskite. A 30 nm-thick ITO film deposited by sputtering was chosen as a transparent recombination layer. Then, a perovskite subcell

was deposited on top of the previous structure without exceeding 120 ºC. The $MAPbI_xBr_{3-x}$ perovskite absorber was optimised by a controlled evaporation of MABr on top of a solution processed $MAPbI_3$ film. Finally, a 1.72 eV bandgap perovskite was found to perform better, giving rise to a perovskite/CIGS monolithic tandem device of 10.98% efficiency. However, this performance is lower than the ones measured for the stand-alone subcells due to the 70-80% transmittance of the Ca/BCP-based front contact. Despite this low efficiency, this work constitutes the unique proof of concept of a two-terminal perovskite/CIGS tandem solar cell. It is necessary to find more convenient recombination layers to supress the ZnO-perovskite chemical contact. In addition, highly transparent conducting materials as AgNWs or TCOs, should be considered as front contacts as it has been successfully done in perovskite/Si tandems.

Type	Device architecture Top cell Bottom cell	J_{sc} ($mA \cdot cm^{-2}$)	V_{oc} (V)	FF	Efficiency (%)	Size (cm^2)	Reference (year)
2T	**Ca/BCP/PCBM/$MAPbI_xBr_{3-x}$/PEDOT:PSS/ITO** **CdS/CIGS/Mo/Si_3N_4**	**12,7**	**1,45**	**0,566**	**10,9**	**0,40**	**96 (2015)**
4T	LiF/FTO/TiO_2/mpTiO_2-$MAPbI_3$/Spiro/AgNWs/LiF CIGS	17.5 10.9	1.025 0.682	0.710 0.788	12.7 5.9	0.39 0.39	85 (2014)
4T	FTO/TiO_2/$MAPbI_3$/Spiro/AgNWs AgNWs/AZO/i-Zno/CdS/CIGS/Mo	17.2 11.2	0.892 0.500	0.540 0.446	8.3 2.5	0.25 0.25	97 (2016)
4T	FTO/TiO_2/mpTiO_2-$MAPbI_3$/Spiro/MoO_3/ZnO:Al ZnO/ZnO:Al/CdS/CIGS/Mo	16.7 14.4	1.034 0.661	0.703 0.774	12.1 7.4	0.28 -	98 (2015)
4T	MoOx/Au/Ag/MoOx//Spiro/$MAPbI_3$/TiO_2/ITO ITO/CdS/CIGS/Mo	14.6 10.2	1.050 0.560	0.751 0.696	11.5 4.0	0.11 -	99 (2015)
4T	FTO/ZnO/PCBM/$MAPbI_3$/Spiro/MoO_3/In_2O_3:H i-ZnO/ZnO:Al/CdS/CIGS/Mo	17.4 12.7	1.104 0.667	0.736 0.749	14.1 6.3	0.52 0.21	100 (2015)
4T	**ZnO:Al/ZnO/PCBM/$MAPbI_3$/PTAA/In_2O_3:H** **i-ZnO/ZnO:Al/CdS/CIGS/Mo**	**19.1** **12.1**	**1.116** **0.669**	**0.754** **0.736**	**16.1** **6.0**	**0.29** **0.21**	**101 (2016)**
4T	FTO/TiO_2/mpTiO_2-$MAPbI_3$/Spiro/Ag/ITO ITO/CdS/CIGS/Mo	20.1 15.2	0.975 0.470	0.781 0.646	15.3 4.6	0.09 0.09	102 (2017)
2T	Al/PCBM/$MAPbI_3$/PEDOT CdS-ITO/CZTS/Mo	5,6	1,353	0,604	4,6	0,45	103 (2014)
4T (opt)	ITO/Poly-TPD/$FA_{0.9}Cs_{0.1}PbI_{2.1}Br_{0.9}$/PCBM/BCP/Ag Al/ZnO:Al/i-ZnO/CdS/CZTS/Mo	18.1 9.01	1.120 0.353	0.720 0.515	14.5 1.6	-	104 (2017)

Table 2. Perovskite/chalcogenide tandem devices reported in the literature. Double junction architecture as well as short circuit current (J_{sc}), open circuit voltage (V_{oc}), fill factor (FF), efficiency, and active area of the devices are summarized. 2T, 4T and 4T (opt) refer to two terminal, mechanically stacked four terminal and optically coupled four terminal architectures, respectively. Words highlighted in blue and red correspond to transparent contacts and recombination layers, respectively. Bold rows point out the record devices for each configuration.

Four-terminal CIGS-based devices. In contrast with the monolithic architecture, there are several reports demonstrating four-terminal perovskite/CIGS solar cell. Bailie and co-authors employed AgNWs as back contact to attain a highly transparent perovskite based subcell. When combined with a 17% CIGS rear subcell, the overall efficiency is boosted up to 18.6% (see Figures 6a and 6c).[85] Later, Lee et al. employed

AgNWs with the same purpose but in a full solution processed version of the $MAPbI_3$/CIGS device.[97] This approach, although cost-effective, yields efficiencies of merely 10%. Albeit, the use of AgNWs in perovskite-based devices is still challenging since the processing is complicated and involve solvents that lead to a large variability of the device performance. In order to find an alternative, a couple of articles were simultaneously published in June 2015 by Tiwari's and Yang's groups.[98,99] The former proposed a sputtered TCO based on ZnO:Al while the latter developed a dielectric-metal-dielectric (DMD) structure based on MoO_x/Au/Ag/MoO_x, as transparent contacts. The complete device structures are FTO/TiO_2/$MAPbI_3$/Spiro/MoO_3/ZnO:Al+CIGS and DMD/Spiro-OMeTAD/$MAPbI_3$/TiO_2/ITO+CIGS, yielding overall efficiencies of 19.5% and 15.5%, respectively. The group of Tiwari has further explored this configuration.[100,101] First, In_2O_3:H was used as high mobility TCO due to its enhanced visible and NIR transmittance, and its high thermal and chemical stability. Moreover, the damage produced to the Spiro-OMeTAD while the ion bombardment is mitigated with respect to the ZnO:Al case. All these benefits give rise to a four-terminal $MAPbI_3$/CIGS tandem solar cell reaching 20.5% efficiency.[100] Then, the combination of ZnO:Al and In_2O_3:H as front and rear contacts, respectively, boosted the performance up to a stabilised 22.1%.[101] Finally, very recently, Guchhait et al. demonstrated a triple cation perovskite based semitransparent device, with an Ag/ITO back contact, that combined with CIGS in a four-terminal configuration yields 20.7%.[102]

CZTSSe-based devices. Beyond CIGS, other chalcogenide solar cells, in particular kesterite (CZTSSe), represent an interesting partner for perovskite materials in tandem applications. Their earth-abundant character, low-temperature processing and 1.1 eV bandgap make kesterites solar cells adequate for harvesting light in the bottom subcell. Todorov et al. firstly evaluated a monolithic perovskite/kesterite tandem solar cell in which a $MAPbI_3$ solar cell was directly deposited on top of a CZTSSe device.[103] The system was affected by a great parasitic absorption since a poorly transparent 25 nm thick Al layer was employed as front contact. Consequently, this proof of concept of chalcogenide-perovskite monolithic architecture performed a low efficiency of 4.6%.[103] In contrast, Li et al. has recently proposed a novel strategy in which the perovskite subcell acts as optical splitter itself.[104] In this design, sunlight reaches a $FA_{0.9}Cs_{0.1}PbI_{2.1}Br_{0.9}$ perovskite solar cell that harvest light up to λ =730 nm while longer wavelengths are reflected by its Ag back contact to be converted to electrical power by a CZTSSe solar cell. The complete four-terminal device has been demonstrated to achieve a 16% efficiency.[104]

Perovskite/perovskite

The first report proposing an all-perovskite based tandem design was published in 2014 by Chen et al.[105] This theoretical work studied from an optical point of view the potential of using $MAPbI_3$ as active layer in both top and bottom cells. However, the lack of optical constants of perovskite materials limited the optical design of all perovskite tandem devices to $MAPbI_3$. Although the expected performance of this double-junction cell could not surpass the one of a single-junction, the authors claimed that the large V_{oc} achievable, higher than 2 V, could be of great interest for several applications such as water splitting. One year later, a couple of articles demonstrated experimentally such theoretical predictions.[106,107] Jiang et al. employed a mesoporous perovskite solar cell in which the fabrication sequence was stopped after the deposition of the perovskite film. Then, a complex recombination layer was deposited by stacking Spiro-OMeTAD, PEDOT:PSS, PEI and PCBM films. The use of orthogonal solvents and dry-transfer methods impeded the degradation of the pre-deposited perovskite underneath. Finally, a $MAPbI_3$-based planar top-cell was constructed on top of the system, resulting in a high-voltage tandem device with V_{oc}=1.89.[107] On the other hand, Heo et al. went a step further making use of a high bandgap (2.25 eV) $MAPbBr_3$ perovskite as active material in the top subcell, in order to push the V_{oc} up to 2.2 V in the double-junction device.[106] In this case, the authors sandwiched a FTO/TiO_2/$MAPbBr_3$/wet-PTAA top subcell and a PCBM/$MAPbI_3$/PEDOT:PSS/ITO bottom subcell. More recently, Forgács et al. achieved monolithic $FA_{0.85}Cs_{0.15}PbI_{0.9}Br_{2.1}$/$MAPbI_3$ tandem solar cells by combining solution process and dual source vapour deposition techniques to construct the front and rear subcells, respectively.[108] The recombination interlayer is made of doped organic semiconductors, TaTm/p-doped TaTm/n-doped C60/C60, whose high conductivity and transparency are controlled thanks to thermal evaporation that, furthermore, assures their compatibility with the underlying perovskite material (see Figure 7a). The resulting device presents a small hysteresis and good reproducibility with average V_{oc} > 2.13 V and matched J_{sc} > 9 mA·cm^{-2}, which yields to an efficiency close to 15%, and a 18% record device (see Figures 7b and 7c).[108]

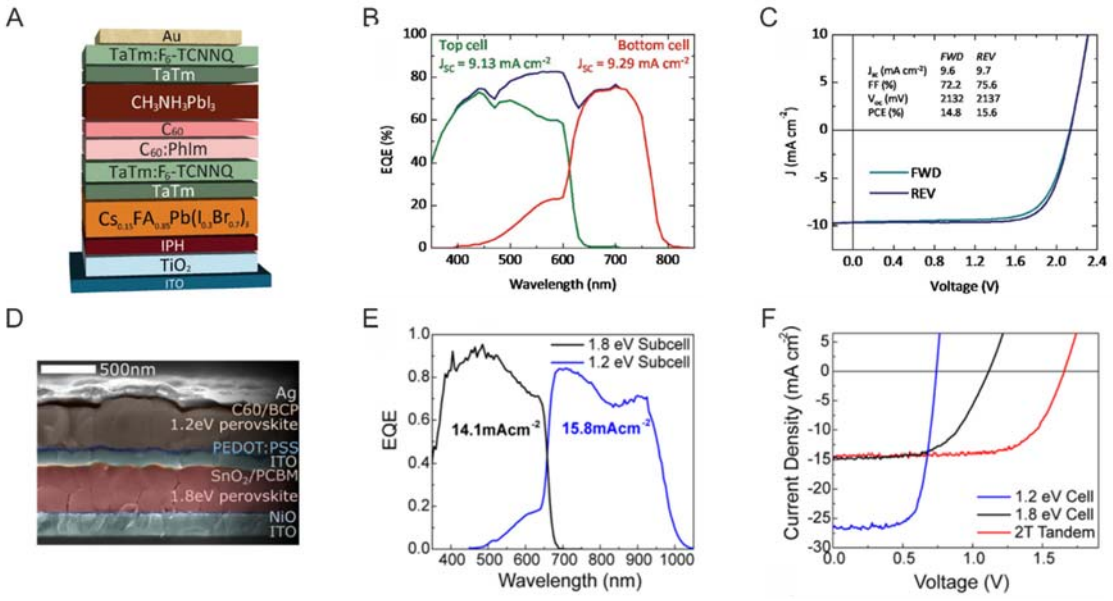

Figure 7. Two terminal perovskite/perovskite tandem solar cells Structure (a), EQE spectra (b) and J-V curve (c) of a device where doped organic semiconductors are employed as charge selective contacts and recombination layers (Adapted with permission of John Wiley & Sons Ltd from Reference 108). SEM cross section image (d), EQE spectra (e) and J-V curve (f) of the record monolithic perovskite/perovskite where the bottom subcell is based on a low bandgap tin rich perovskite. From Reference 34. Reprinted with permission from AAAS.

The aim of using all-perovskite tandem devices as a straight path for the generalize use of third-generation PV technology requires to enhance the efficiencies closer to the ones of Si cells. The approaches previously reviewed, although reporting extraordinary voltages, present moderate efficiencies that will be hardly improved due to the limited solar spectrum range covered by the Pb-based perovskites (400-to-820 nm). So far, the partial substitution of the Pb cation by Sn is the most compelling way to shift the bandgap the of perovskite material towards the infrared region.[19] Thus, $APb_{1-x}Sn_xI_3$ compounds are capturing the attention of the community for their application in highly efficient perovskite-on-perovskite tandem solar cells. In June 2016, Anaya et al. followed a solvent engineering/anti-solvent method to prepare $MAPb_{1-x}Sn_xI_3$ films that were structural and optically stable.[30] These features allowed extracting their complex refractive index for the first time, and evaluating the impact of mixed Pb-Sn perovskites in the eventual performance of realistically simulated tandem devices. Although an achievable efficiency of 34% was theoretically found for a $MAPb_{0.15}Sn_{0.85}I_3/MAPbI_3$ system,[30] chemical instabilities related to the Sn^{2+} oxidation to Sn^{4+} states prevented the experimental demonstration of efficiencies close to the values therein predicted. In order to alleviate the Sn^{2+} oxidation, Yang et al. added FA cations to attain $FA_{0.5}MA_{0.5}Pb_{0.75}Sn_{0.25}I_3$ with a 1.33 eV bandgap that yielded to single-junction solar cells showing stabilized PCE of 14.19%.[109] When this material is combined with a $MAPbI_3$ top subcell in a four-terminal double-junction-like architecture, the complete device gives rise to a record PCE of 19.08%.[109]

Soon after, Eperon et al. reported for the first time a perovskite-on-perovskite monolithic tandem solar cell in which the rear subcell is based on a low bandgap Sn-perovskite.[34] First, they demonstrated that the use of Cs improved the short circuit current of Sn-based perovskite solar cells significantly. Indeed, a 1.22 eV bandgap $FA_{0.75}Cs_{0.25}Pb_{0.5}Sn_{0.5}I_3$ perovskite-based device showed an outstanding 14.8% (26.7 $mA \cdot cm^{-2}$) compared with the 10.9% obtained for the $FAPb_{0.5}Sn_{0.5}I_3$-based one. Then, they prepared a monolithically integrated $FA_{0.83}Cs_{0.17}PbI_{1.5}Br_{1.5}$/ $FA_{0.75}Cs_{0.25}Pb_{0.5}Sn_{0.5}I_3$ tandem solar cell in which ITO was deposited by sputtering and employed as recombination layer (see Figure 7d). The device featured a matched J_{sc} of 14.1 $mA \cdot cm^{-2}$ that resulted in a very promising 17.0% stabilized PCE (see Figures 7e and 7f). A $FA_{0.83}Cs_{0.17}PbI_{2.49}Br_{0.51}$/ $FA_{0.75}Cs_{0.25}Pb_{0.5}Sn_{0.5}I_3$ four-terminal system was also demonstrated with 20.3% efficiency.[34] This latter result has been surpassed very recently in a paper by Zhao et al. where a 21.0% efficiency 4-terminal $FA_{0.3}MA_{0.7}PbI_3$/ $FA_{0.6}MA_{0.4}Pb_{0.4}Sn_{0.6}I_3$ device was reported.[67] Finally, during the writing process of this review, Rajagopa *et al.* have reported an integrated process that combines compositional, interfacial, optical and device engineering to demonstrate a 18.5% two terminal perovskite on perovskite tandem device. The measured photovoltage represents 80% of the theoretical limit, which is the lowest among all the perovskite-based tandem solar cells.[110]

It is reasonable to foresee that more advances related to all-perovskite tandem cells will come in the very near future, as may researchers are focusing on finding ways to overcome the obstacles herein described, motivated by the enormous potential such devices hold in terms of high efficiency and low cost. Next efforts should focus on improving the stability of low-bandgap perovskites under working conditions, and the production of more favourable ESLs and HSLs in terms of band alignment. In this regard, combining low bandgap perovskite materials, like the ones reported in Ref 34, and deposition methods and doped organic semiconductors as proposed in Ref. 108, may pave the way to the demonstration of perovskite-on-perovskite devices approaching 30% efficiencies.

Perovskite/Polymer

Polymer solar cells are good candidates to be combined with perovskite devices to form tandem architectures since they share interlayers and they are processed by similar methods. Moreover, the chemical versatility of both organic and perovskite absorbers allows tuning their bandgaps in a simple way. Chen et al. employed a new IR-polymer (PBSeDTEG8) and $MAPbI_3$ to make the top and the bottom subcells, respectively, that yield a 10.23% monolithic tandem device.[111] The polymer employed had excellent thermal tolerance in order to avoid its degradation with the perovskite thermal treatment. Later,

Liu et al. turned over the design and integrated the perovskite material as front subcell to prevent polymer deterioration with thermal annealing.[112] This approach, where PCE-10:$PC_{71}BM$ is employed as light harvester in the polymer subcell, led to 16.0% two-terminal tandem solar cells. The slight increment in performance in comparison to the one of the stand-alone perovskite solar cell (15.6%) is compensated by the benefit of employing less amount of Pb in the double-junction structure.[112] It seems that the utilisation of alternative solution processes that imply low-temperature annealing,[113,114] or high-vacuum techniques,[43,44] to deposit the perovskite material may mitigate the thermal decomposition of the polymer and, thus, allow the fabrication of organic/perovskite tandem devices of superior performances.

Type	Device architecture Top cell Bottom cell	J_{sc} ($mA \cdot cm^{-2}$)	V_{oc} (V)	FF	Efficiency (%)	Size (cm^2)	Reference (year)
2T	FTO/TiO_2/$MAPbBr_3$/PTAA PCBM/$MAPbI_3$/PEDOT:PSS/ITO	8,3	2,250	0,560	10,4	0,10	106 (2016)
2T	PEDOT:PSS/Spiro/$MAPbI_3$/PCBM/PEI PEDOT:PSS/Spiro/m$pTiO_2$-$MAPbI_3$/TiO_2/FTO	6,6	1,890	0,560	7,0	0,10	107 (2016)
2T	ITO/IPH/$FA_{0.85}Cs_{0.15}PbI_{0.9}Br_{2.1}$/TaTm/TaTm:F6-TCNNQ C60:PhIm/C60/$MAPbI_3$/TaTm/TaTm:F6-TCNNQ/Au	9,8	2,294	0,803	18,1	0,03	108 (2017)
4T	ITO/NiO_x/$MAPbI_3$/PCBM/C60/ITO ITO/PEDOT:PSS/$FA_{0.5}MA_{0.5}Pb_{0.75}Sn_{2.1}I_3$/PCBM/C60/Ag	16.7 9.1	1.080 0.760	0.750 0.800	13.5 5.6	0.03 0.03	109 (2016)
2T	ITO/NiO/$FA_{0.83}Cs_{0.17}PbI_{1.5}Br_{1.5}$/$SnO_2$-PCBM/ITO PEDOT:PSS/$FA_{0.75}Cs_{0.25}Pb_{0.5}Sn_{0.5}I_3$/C60-BCP/Ag	14,5	1,660	0,700	16,9	0,20	34 (2016)
4T	ITO/NiO/$FA_{0.83}Cs_{0.17}Pb(I_{0.83}Br_{0.17})_3$/$SnO_2$-PCBM/ITO ITO/PEDOT:PSS/$FA_{0.75}Cs_{0.25}Pb_{0.5}Sn_{0.5}I_3$/C60-BCP/Ag	20.3 7.9	0.970 0.740	0.790 0.730	15.7 4.4	0.20 0.20	34 (2016)
4T	**MoO_x/Au/MoO_x/Spiro/$FA_{0.3}MA_{0.7}PbI_3$/C60/SnO_2/FTO ITO/PEDOT:PSS/$FA_{0.6}MA_{0.7}Pb_{0.4}Sn_{0.6}I_3$/C60-BCP/Ag**	**20.1 4.8**	**1.141 0.808**	**0.800 0.744**	**18.3 2.9**	**0.20 0.20**	**67 (2017)**
4T (opt)	FTO/TiO_2/m$pTiO_2$-$MAPbBr_3$/Spiro/Au FTO/TiO_2/$MAPbI_3$/Spiro/Au	7.2 12.1	1.265 0.826	0.720 0.680	6.5 6.9	0.05 0.16	94 (2015)
2T	**ITO/NiO_x/$MA_{0.9}Cs_{0.1}PbI_{1.8}Br_{1.2}$/C60/Bis-C60/ITO PEDOT:PSS/$MAPb_{0.5}Sn_{0.5}I_3$/IC60BA/Bis-C60/Ag**	**12,7**	**1,980**	**0,730**	**18.5**	**0,10**	**110 (2017)**
2T	ITO/PEDOT:PSS/PBSeDTEG8:PCBM/TiO_2/PEDOT:PSS-PH500 PEDOT:PSS-4083/$MAPbI_3$/PCBM/PFN-Al	10,1	1,520	0,670	10,2	0,10	111 (2015)
2T	**ITO/PEDOT:PSS/$MAPbI_3$/PCBM/MoO_3/Ag/C60-SB PCE-10:PC71BM/C60-n/Ag**	**13,1**	**1,630**	**0,751**	**16,0**	**0,06**	**112 (2016)**

Table 3. Perovskite/perovskite and perovskite/polymer tandem devices reported in the literature. Double junction architecture as well as short circuit current (J_{sc}), open circuit voltage (V_{oc}), fill factor (FF), efficiency, and active area of the devices are summarized. 2T, 4T and 4T (opt) refer to two-terminal, mechanically stacked four-terminal and optically coupled four-terminal architectures, respectively. Words highlighted in blue and red correspond to transparent contacts and recombination layers, respectively. Bold rows point out the record devices for each configuration.

Considerations to develop perovskite based double junction devices of improved efficiency

Different aspects may be addressed in order to drive perovskite based tandem solar cells to superior efficiencies. In this regard, the choice of light harvesters plays the most critical role in the performance of

a tandem device. Similarly to what happens in a single-junction device, pairs of optimum absorption onsets for both top and bottom absorbers can be found according to SQ theory in order to achieve maximized performances. Figure 8a displays the expected efficiency for ideal four-terminal double-junction devices as a function of the E_{bg} of both top and bottom harvesters. For example, the optimal top subcell E_{bg} for a Si bottom subcell is close to 1.7 eV that corresponds to different ABX_3 perovskites families as shown in Figure 3b.[77] Analogously, for a CIS subcell with E_{bg}=1.0 eV, optimal top subcell E_{bg} should be around 1.6 eV. The right selection of bandgaps leads to efficiencies above 40% in the ideal case, which represents a theoretical ceiling. However, other electro-optical considerations must be taken into account in order to design actual devices. All device components need to be designed in order to: i) achieve low resistance (high conductivity) and adequate energy band alignment from the electrical point of view, and ii) minimize both parasitic absorption, which takes place at the substrate, contacts, ESLs and HSLs and reflectance losses from the optical. Additional requirements must be addressed in a monolithic tandem. Since bottom and top subcells are connected in series, the same current density must flow through each subcell in what is normally known as current matching condition for two-terminal tandems. Also, an intermediate layer must be employed in order to assist recombination of non-extracted electrons and holes.

In Figure 8b we show the calculated spectral dependence of the absorptance and reflectance of a device formed by glass/ITO/TiO_2/$FA_{0.83}Cs_{0.17}PbI_{1.8}Br_{1.2}$/Spiro/ITO/$TiO_2$/$MAPb_{0.15}Sn_{0.85}I_3$/Spiro/Au. Each layer thickness has been optimized using a genetic algorithm in order to maximize photocurrent matching. Perovskite layers are restricted to be thinner than 600 nm in order to prevent charge diffusion issues. We have selected ITO, gold, TiO_2 and Spiro as contacts, ESL and HSL, which are the most common materials employed in perovskite devices. The choice of the perovskite compounds is the optimum according to SQ theory (Figure 8a) considering the lowest bandgap perovskite reported (E_{bg}=1.17 eV).[30] We employed a model based on the transfer matrix formalism in which the complex refractive indices of the different materials are taken into account to predict the optical behaviour of the complete device.[21,30] The photogenerated current of the total device is calculated from the fraction of light absorbed by the perovskite material assuming no electrical losses, i.e. IQE=1. It is important to notice that to perform accurate predictions is central to count on a reliable experimental characterization of the optical constants of the different materials involved, which is challenging for ABX_3 perovskites due to the strong dependence of the optical properties with the preparation conditions. We refer the reader to different

articles where this topic is discussed in detail.[21,30,68,115,116,117] In Figure 8c we display the thickness obtained for each layer comprising the tandem device. We also present the photocurrent associated to the fraction of the incident light absorbed at each component. In particular, 4 $mA \cdot cm^{-2}$ and 1 $mA \cdot cm^{-2}$ are wasted by ITO and charge selective contacts, whereas 5 $mA \cdot cm^{-2}$ are lost at the device entrance. Our design yields a photocurrent matching value of 14 $mA \cdot cm^{-2}$, which potentially leads to 30% efficiency. However, ca. 10 $mA \cdot cm^{-2}$ are lost, which indicates there is still room for improvement in the device performance. Hereof, a proper choice of contacts, charge selective layers and antireflective films is of great importance for the demonstration of tandems of superior efficiencies.

Transparent contacts. Ideally, materials employed as transparent contacts should minimize absorption in the 350-to-1200 nm spectral range and sheet resistance to allow both transmittance of light and transport of charge carriers. Regarding the materials comprising the cell described in Figure 8b-c, the front transparent contact is the one leading to higher optical losses. Although ITO is employed for the fabrication of the most efficient perovskite-based tandem solar cells (see Tables 1, 2, and 3), alternative materials have been reported such as FTO, IZO, AgNWs or Au thin film as we have already discussed in section 3. We present in Figure 8d the calculated spectral dependence of the transmittance of each of these layers deposited on a glass substrate assuming optical constants reported elsewhere.[30,118,119] Film thicknesses are the ones that these materials typically feature in order to allow a realistic comparison. Also, Figure 8d displays the photogenerated current loss associated to each material. Notice that, although these results allow comparing the performance of different materials employed as contacts, the actual fraction of the incident light wasted by such contacts in a device requires the full simulation of the complete system. Recent results demonstrate that metal grids of 20-30 μm deposited on top of transparent conductors reduce their sheet resistance while enhancing light transmission.[120] Finally, it is worth to mention that intermediate transparent contacts used in a four-terminal architecture (see Figure 2d-e) require a narrower window of transparency than the front contacts.

As it has been previously discussed in section 3, deposition techniques commonly employed to prepare transparent contacts (ITO, FTO, IZO) could damage perovskite, ESL or HSL layers. This makes necessary to pre-deposit a buffer layer such as MoO_x. or less expensive solution-processed ZnO.[90] Such buffer layers merely show an electrical influence on the device since their very thin character prevents them from having a significant impact in the optical behaviour.

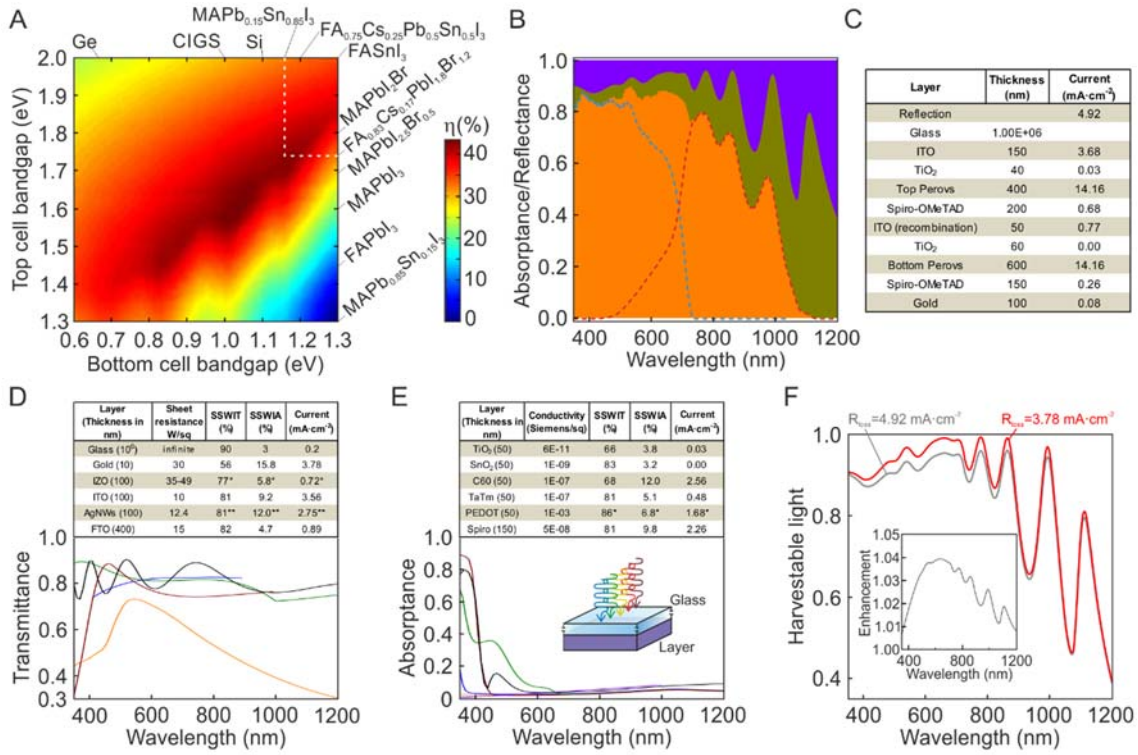

Figure 8. (a) Expected efficiency for ideal double-junction devices as a function of E_{bg} of both top and bottom light harvesters. A selection of well stablished and perovskite absorbers are displayed. (b) Calculated spectral dependence of effective (orange) and parasitic (green) absorptance and reflectance (purple) of a perovskite/perovskite device formed by glass/ITO/TiO_2/$FA_{0.83}Cs_{0.17}PbI_{1.8}Br_{1.2}$/Spiro/ITO/$TiO_2$/$MAPb_{0.15}Sn_{0.85}I_3$/Spiro/Au. Blue and red dashed lines represent light absorbed by the top and bottom perovskite material, respectively. (c) Layout of the device, thickness and current associated to the fraction of the incident light absorbed at each component. (d) Calculated spectral dependence of the transmittance of a selection of transparent contacts: gold (orange), IZO (red), ITO (green), AgNWs (blue) and FTO (black). Sheet resistance, SSWIT, SSWIA and current associated to the fraction of the incident light absorbed at each material are displayed. (e) Calculated spectral dependence of the absorptance of a selection of charge selective layers: TiO_2 (blue), SnO_2 (orange), C60 (green), TaTm (red), PEDOT:PSS (purple) and Spiro-OMeTAD (black). Conductivity, SSWIT, SSWIA and current associated to the fraction of the incident light absorbed at each material are displayed. (f) Calculated spectral dependence of the fraction of the incident light that is harvestable by the device with (red) and without (grey) a SiO_2 based antireflective layer. Inset shows the ratio between the spectral harvestable light with and without antireflective layer. SSWIT=solar spectrum weighted integrated transmittance. SSWIA=solar spectrum weighted integrated absorptance. Calculations are made for wavelengths from 350 nm to 1200 nm, except for * (350-1000) and ** (400-900).

Electron and hole selective layers. Similarly to the previous section, we present in Figure 8e the calculated spectral dependence of the fraction of light absorbed by ESL and HSL materials typically employed in perovskite-based tandems.[30] Thicknesses of the layers are those considered standard in the field. TiO_2 and Spiro-OMeTAD are the most widely used ESL and HSL materials in single junction devices. However, Spiro-OMeTAD presents serious concerns regarding its long term stability. Indeed, none of the recently reported record tandem cells employs this material (see Tables 1, 2 and 3). Our calculations reveal that SnO_2, and PEDOT are very interesting materials for ESL and HSL since they show less absorption than Spiro-OMeTAD while preserving good electrical properties and ease of processing. Nevertheless, although PEDOT features better transparency, it presents instability issues like

Spiro-OMeTAD, thus further improvements in this direction are required. Finally, evaporated organic semiconductors (C60 and TaTm) hold great promise in the field due to their tuneable electro-optical properties by means of doping.[108,121]

Recombination layers. Recombination layers employed in two-terminal architectures are made of materials that have been already reviewed either in the *transparent contacts* or in the *electron and hole selective layers* sections. Thus, optical considerations can be directly applied for them. Regarding electrical properties, they have less restrictive preconditions than contacts since they just may ensure charge diffusion in the direction perpendicular to the stacking of layers.

Reflection losses. Light reflected at the entrance of the system represents half of the light that cannot be harvested in the device (Figure 8c). Reflection losses are caused by the sudden change in the refractive index perceived by the light beam when passing from one medium to another, in this case from air (n=1) to glass (n=1.51). Designing optimized antireflective layers that work throughout the operational spectral range represents a big challenge. Here we propose a very simple example that consists on a porous SiO_2 layer of 100 nm on top of the glass substrate to enhance the incident light in-coupling. This layer can be prepared using cost-effective SiO_2 nanoparticles that are easily processable and large scale amenable by solution processing.[122] Such antireflective coating makes an extra 1 $mA \cdot cm^{-2}$ available to be extracted from the solar cell as shown in Figure 8f.

Future lines

In what follows, we share our view on the avenues the perovskite community may take in the near future to push perovskite-based tandem devices to further horizons. We also provide the reader with some of the exploratory alternatives that are being incipiently investigated.

Stability and scalability of perovskite solar cells. The stability of perovskite materials must reach values comparable to those associated to Silicon or CIGS PV technologies if perovskite-based tandems are pursued. This means, regardless their composition, perovskites should satisfy a 25 years life under operation without degrading the efficiency more than a 20% in module configuration. These requirements are less stringent for niche markets such as building integrated or flexible PV. Thermal and moisture stability of the perovskite need to be enhanced by chemical management and proper device encapsulation as, for instance, Bella *et al.* demonstrate in Reference 123. Finally, notice that inkjet printing,[124] and slot-

die coupled to roll-to-roll processes[125,126] have been pointed out to play a key role in the scaling up process of perovskite solar modules, and thus in tandem technology.

Stable high bandgap perovskites. Perovskites in which iodide is partially substituted by bromide feature optimal absorption onsets for topcells that are combined with Si- or CIGS-based bottom subcells (see Figure 8a). However, phase segregation takes place in the material under illumination which is harmful for the device. Significant efforts in the development of perovskites with A site containing Cs^+ have been made in order to decrease the Goldschmidt tolerance factor and thus stabilize the structure.[60] Another strategy consists on the development of films of enlarged perovskite grains with the aim of reducing the number of boundaries where ion-migration mainly occurs.[127]

Stable low bandgap perovskite. Nowadays, tin based perovskites represent a unique strategy in order to reduce the bandgap of ABX_3 semiconductors towards the near infrared. Nevertheless, Sn^{2+} present in the material oxidizes easily to Sn^{4+}, which is detrimental for the consecution of a working device. Both the addition of FA^+ and Cs^+ cations, and the use of a tin compensator/reducing agent, usually based on SnF_2, are promising paths to overcome the ambient instability of these tin rich perovskites.[55]

Perovskite materials with E_{bg}<1.17 eV. Hitherto, the lowest bandgap achievable is E_{bg}=1.17 eV, when $MAPb_{0.15}Sn_{0.85}I_3$ is used.[30] The development of ABX_3 perovskites enabling the absorption of photons with wavelengths larger than 1100 nm would suppose a breakthrough in the field. In particular, materials with E_{bg}=1.0 eV would be ideal for double-junction devices. A further decrease in the E_{bg} of the ABX_3 compound will open paths towards the creation of triple-junction all-perovskite devices. In this regard, larger A-site cations may be explored in order to further decrease the bandgap of the perovskite absorber, which requires exploring the limits of the Goldschmidt tolerance factor.[128]

Triple junction perovskite solar cells. Triple- or more-junction designs will allow the development of solar cells in which a larger fraction of photons can be harvested minimizing voltage losses. In another note, as pointed out in Ref. 129, the combination of E_{bg} of 2.06 eV/1.55 eV/1.17 eV, which are nowadays achievable with perovskite materials, results optimum for ultra-high solar concentration systems.

Light management. Perovskite materials are highly efficient absorbers. For this reason, in general it is not necessary to develop light management strategies to improve light absorption in single junction devices. Of course, due to environmental concerns, optimization of the optical design of the single junction device

may still be required to preserve optical absorption while reducing the amount of the lead base absorber.[117] However, such approaches may become relevant merely from the perspective of efficiency in tandem solar cells. Indeed, as a transparent (non-reflective) layer is deposited over the active layer of the top subcell, a fraction the light harvestable by the perovskite front layer does not have a second chance to be absorbed in contrast of what would happen if a metallic contact were used. In the particular case of a two-terminal device, it is not possible to make use of the light emitted as a result of radiative recombination in the layer between subcells. In all cases, optical strategies such as photonic crystals,[130,131,132] metamaterials,[133] surface textures,[134,135] light scatterers[136] or metallic nanostructures exhibiting plasmonic resonances[117] can be used to provide the device with an efficient photon delivery. Also, photonic architectures could be considered if an accurate control of the angular dependence of the absorbed light is needed.

Acknowledgments

The research leading to these results has received funding from the European Research Council under the European Union's Seventh Framework Programme (FP7/2007-2013)/ERC grant agreement n° 307081 (POLIGHT), the Spanish Ministry of Economy and Competitiveness under grant MAT2014-54852-R. MA is grateful to "La Caixa" Foundation for its financial support. The authors declare no competing financial interest.

Author contributions

All authors contributed to the discussion and writing of the manuscript.

References

1 European Comission (2015). Paris Agreement, 21st Conference of the Parties.

2 International Energy Agency (2016). World Energy Outlook 2016.

3 Perez, R., and Perez, M. (2015). A fundamental look at supply side energy reserves for the planet. The IEA SHC Solar Update 62, 4–6.

4 Result of the search 'PV and solar cell' in the Web of Science.

5 World Economic Forum (2016). Top 10 Emerging Technologies of 2016.

6 Kojima, A., Teshima, K., Shirai, Y., and Miyasaka, T. (2009). Organometal halide perovskites as visible-light sensitizers for photovoltaic cells. J Am Chem Soc. 131, 6050–6051.

7 Correa-Baena, J-P., Abate, A., Saliba, M., Tress, W., Jacobsson, T. J., Grätzel, M., and Hagfeldt, A. (2017). The rapid evolution of highly efficient perovskite solar cells. Energy Environ. Sci. 10, 710–727.

8 NREL chart.

9 Green, M. A., Emery, K., Hishikawa, Y., Warta, W., Dunlop, E. D., Levi, D. H., Hohl-Ebinger, J., and Ho-Baillie, A. W. Y. (2017). Solar cell efficiency tables (version 50). Prog. Photovolt. Res. Appl. 25, 668–676.

10 Shockley, W., and Queisser, H. J. (1961). Detailed balance limit of efficiency of p-n junction solar cells. J Appl Phys. 32, 510–519.

11 Li, M., Bhaumik, S., Goh, T. W., Kumar, M. S., Yantara, N., Grätzel, M., Mhaisalkar, S., Mathews, N., and Sum, T. C. (2017). Slow cooling and highly efficient extraction of hot carriers in colloidal perovskite nanocrystals. Nat. Commun. 8, 14350.

12 Guo, Z., Wan, Y., Yang, M., Snaider, J., Zhu, K., and Huang, L. (2017). Long-range hot-carrier transport in hybrid perovskites visualized by ultrafast microscopy. Science 356, 59–62.

13 Vogel, D. J., Kryjevski, A., Inerbaev, T. M., and Kilin, D. S. (2017). Photoinduced single- and multiple- electron dynamics processes enhanced by quantum confinement in lead halide perovskite quantum dots. J. Phys. Chem. Lett. 8, 3032-3039.

14 Yu, Z., Leilaeioun, M., and Holman, Z. (2016). Selecting tandem partners for silicon solar cells. Nat. Energy. 1, 16137.

15 Tanabe, K. (2009). A review of ultrahigh efficiency III-V semiconductor compound solar cells: Multijunction tandem, lower dimensional, photonic up/down conversion and plasmonic nanometallic structures. Energies 2, 504–530.

16 Ameri, T., Li, N., and Brabec, C. J. (2013). Highly efficient organic tandem solar cells: a follow up review. Energy Environ. Sci. 6, 2390.

17 Torchynska, T. V., and Polupan, G. (2004). High efficiency solar cells for space applications. Superf. Vacío 17, 21–25.

18 Onoda-Yamamuro, N., Matsuo, T., and Suga, H. (1992). Dielectric study of $CH_3NH_3PbX_3$ (X = Cl, Br, I). J. Phys. Chem. Solids. 53, 935–939.

19 Stoumpos, C. C., Malliakas, C. D., and Kanatzidis, M. G. (2013). Organic tin and lead iodide perovskites with organic cations : unique semiconductors , with phase transitions and near-infrared photoluminescent properties. Inorg. Chem. 52, 9019–9038.

20 Baikie, T., Fang, Y., Kadro, J. M., Schreyer, M., Wei, F., Mhaisalkar, S. G., Graetzel, M., and White, T. J. (2013). Synthesis and crystal chemistry of the hybrid perovskite $(CH_3NH_3)PbI_3$ for solid-state sensitised solar cell applications. J. Mater. Chem. A. 1, 5628–5641.

21 Anaya, M., Lozano, G., Calvo, M. E., Zhang, W., Johnston, M. B., and Snaith, H. J. (2015). Optical description of mesostructured organic-inorganic halide perovskite solar cells. J. Phys. Chem. Lett. 6, 48–53.

22 Miyata, A., Mitioglu, A., Plochocka, P., Portugall, O., Wang, J. T.-W., Stranks, S. D., Snaith, H. J., and Nicholas, R. J. (2015). Direct measurement of the exciton binding energy and effective masses for charge carriers in organic-inorganic tri-halide perovskites. Nat. Phys. 11, 582–587.

23 Stranks, S. D., Eperon, G. E., Grancini, G., Menelaou, C., Alcocer, M. J. P., Leijtens, T., Herz, L. M., Petrozza, A., and Snaith, H. J. (2014). Electron-hole diffusion lengths exceeding Micrometer in an Organometal Trihalide Perovskite Absorber. Science. 342, 341–344.

24 Deschler, F., Price, M., Pathak, S., Klintberg, L. E., Jarausch, D., Higler, R., Hu, S., Leijtens, T., Stranks, S. D., Snaith, H. J., et al. (2014). High photoluminescence efficiency and optically pumped lasing in solution-processed mixed halide perovskite semiconductors. J. Phys. Chem. Lett. 5, 1421–1426.

25 Xing, G., Mathews, N., Lim, S. S., Yantara, N., Liu, X., Sabba, D., Grätzel, M., Mhaisalkar, S., and Sum, T. C. (2014). Low-temperature solution-processed wavelength-tunable perovskites for lasing. Nat. Mater. 13, 476–480.

26 Tan, Z.-K., Moghaddam, R. S., Lai, M. L., Docampo, P., Higler, R., Deschler, F., Price, M., Sadhanala, A., Pazos, L. M., Credgington, D., et al. (2014). Bright light-emitting diodes based on organometal halide perovskite. Nat. Nanotechnol. 9, 687–692.

27 Cho, H., Jeong, S., Park, M., Kim, Y., Wolf, C., Lee, C., Heo, J. H., Sadhanala, A., Myoung, N., Yoo, S., et al. (2015). Overcoming the electroluminescence efficiency limitations of perovskite light-emitting diodes. Science 350, 1222–1225.

28 Noh, J. H., Im, S. H., Heo, J. H., Mandal, T. N., and Seok, S. I. (2013). Chemical management for colorful, efficient, and stable inorganic-organic hybrid nanostructured solar cells. Nano Lett. 13. 1764–1769.

29 Sadhanala, A., Ahmad, S., Zhao, B., Giesbrecht, N., Pearce, P. M., Deschler, F., Hoye, R. L. Z., Gödel, K. C., Bein, T., Docampo, P., et al. (2015). Blue-green color tunable solution processable organolead chloride-bromide mixed halide perovskites for optoelectronic applications. Nano Lett. 15, 6095–6101.

30 Anaya, M., Correa-Baena, J. P., Lozano, G., Saliba, M., Anguita, P., Roose, B., Abate, A., Steiner, U., Grätzel, M., Calvo, M. E., et al. (2016). Optical analysis of $CH_3NH_3Sn_xPb_{1-x}I_3$ absorbers: a roadmap for perovskite-on-perovskite tandem solar cells. J. Mater. Chem. A 4, 11214–11221.

31 Jacobsson, T. J., Correa-Baena, J.-P., Pazoki, M., Saliba, M., Schenk, K., Grätzel, M., and Hagfeldt, A. (2016). Exploration of the compositional space for mixed lead halogen perovskites for high efficiency solar cells. Energy Environ. Sci. 9, 1706–1724.

32 Eperon, G. E., Stranks, S. D., Menelaou, C., Johnston, M. B., Herz, L. M., and Snaith, H. J. (2014). Formamidinium lead trihalide: a broadly tunable perovskite for efficient planar heterojunction solar cells. Energy Environ. Sci. 7, 982–988.

33 Levchuk, I., Osvet, A., Tang, X., Brandl, M., Perea, J. D., Hoegl, F., Matt, G. J., Hock, R., Batentschuk, M., and Brabec, C. J. (2017). Brightly luminescent and color-tunable formamidinium lead halide perovskite $FAPbX_3$ (X = Cl, Br, I) Colloidal Nanocrystals. Nano Lett. 17, 2765–2770.

34 Eperon, G. E., Leijtens, T., Bush, K. A., Prasanna, R., Green, T., Wang, J. T.-W., Mc Meekin, D. P., Volonakis, G., Milot, R. L., May, R., et al. (2016). Perovskite-perovskite tandem photovoltaics with optimized band gaps. Science 354, 861–865.

35 Li, Z., Yang, M., Park, J. S., Wei, S. H., Berry, J. J., and Zhu, K. (2016). Stabilizing perovskite structures by tuning tolerance factor: formation of formamidinium and cesium lead iodide solid-state alloys. Chem. Mater. 28, 284–292.

36 Protesescu, L., Yakunin, S., Bodnarchuk, M. I., Krieg, F., Caputo, R., Hendon, C. H., Yang, R. X., Walsh, A., and Kovalenko, M. V. (2015). Nanocrystals of cesium lead halide perovskites ($CsPbX_3$, X = Cl, Br, and I): novel optoelectronic materials showing bright emission with wide color gamut. Nano Lett. 15, 3692–3696.

37 Lee, M. M., Teuscher, J., Miyasaka, T., Murakami, T. N., and Snaith, H. J. (2012). Efficient hybrid solar cells based on meso-superstructured organometal halide perovskites. Science 338, 643–647.

38 Burschka, J., Pellet, N., Moon, S-J., Humphry-Baker, R., Gao, P., Nazeeruddin, M. K., and Grätzel, M. (2013). Sequential deposition as a route to high-performance perovskite-sensitized solar cells. Nature. 499, 316–320.

39 Xiao, M., Huang, F., Huang, W., Dkhissi, Y., Zhu, Y., Etheridge, J., Gray-Weale, A., Bach, U., Cheng, Y. B., and Spiccia, L. (2014). A fast deposition-crystallization procedure for highly efficient lead iodide perovskite thin-film solar cells. Angew. Chemie Int. Ed. 53, 9898–9903.

40 Jeon, N. J., Noh, J. H., Kim, Y. C., Yang, W. S., Ryu, S., and Seok, S. I. (2014). Solvent engineering for high-performance inorganic-organic hybrid perovskite solar cells. Nat. Mater. 13, 1–7.

41 Huang, L., Li, C., Sun, X., Xu, R., Du, Y., Ni, J., Cai, H., Li, J., Hu, Z., and Zhang, J. (2017). Efficient and hysteresis-less pseudo-planar heterojunction perovskite solar cells fabricated by a facile and solution-saving one-step dip-coating method. Org. Electron. Physics Mater. Appl. 40, 13–23.

42 Das, S., Yang, B., Gu, G., Joshi, P. C., Ivanov, I. N., Rouleau, C. M., Aytug, T., Geohegan, D. B., and Xiao, K. (2015). High-performance flexible perovskite solar cells by using a combination of ultrasonic spray-coating and low thermal budget photonic curing. ACS Photonics 2, 680–686.

43 Liu, M., Johnston, M. B., and Snaith, H. J. (2013). Efficient planar heterojunction perovskite solar cells by vapour deposition. Nature 501, 395–398.

44 Malinkiewicz, O., Yella, A., Lee, Y. H., Espallargas, G. M. M., Graetzel, M., Nazeeruddin, M. K., and Bolink, H. J. (2014). Perovskite solar cells employing organic charge-transport layers. Nat. Photonics. 8, 128–132.

45 Leyden, M. R., Ono, L. K., Raga, S., Kato, Y., Wang, S., Qi, Y. (2014). High performance perovskite solar cells by hybrid chemical vapor deposition. J. Mater. Chem. A 2, 18742-18745.

46 Raga, S., Ono, L. K., and Qi, Y. (2016). Rapid perovskite formation by CH_3NH_2 gas-induced intercalation and reaction of PbI_2. J. Mater. Chem. A 4, 2494-2500.

47 Brandt, R. E., Stevanović, V., Ginley, D. S., and Buonassisi, T. (2015). Identifying defect-tolerant semiconductors with high minority-carrier lifetimes: beyond hybrid lead halide perovskites. MRS Commun. 5, 265–275.

48 Stoumpos, C. C., Frazer, L., Clark, D. J., Kim, Y. S., Rhim, S. H., Freeman, A. J., Ketterson, J. B., Jang, J. I., and Kanatzidis, M. G. (2015). Hybrid germanium iodide perovskite semiconductors: Active lone pairs, structural distortions, direct and indirect energy gaps, and strong nonlinear optical properties. J. Am. Chem. Soc. 137, 6804–6819.

49 Noel, N. K., Stranks, S. D., Abate, A., Wehrenfennig, C., Guarnera, S., Haghighirad, A.-A., Sadhanala, A., Eperon, G. E., Pathak, S. K., Johnston, M. B., et al. (2014). Lead-free organic–inorganic tin halide perovskites for photovoltaic applications. Energy Environ. Sci. 7, 3061–3068.

50 Hao, F., Stoumpos, C. C., Cao, D. H., Chang, R. P. H., and Kanatzidis, M. G. (2014). Lead-free solid-state organic–inorganic halide perovskite solar cells. Nat. Photonics. 8, 489–494.

51 Hao, F., Stoumpos, C. C., Chang, R. P. H., and Kanatzidis, M. G. (2014). Anomalous band gap behavior in mixed Sn and Pb perovskites enables broadening of absorption spectrum in solar cells. J. Am. Chem. Soc. 136, 8094–8099.

52 Jacobsson, T. J., Pazoki, M., Hagfeldt, A., and Edvinsson, T. (2015). Goldschmidt rules and strontium replacement in lead halogen perovskite solar cells: theory and preliminary experiments on $CH_3NH_3SrI_3$. J. Phys. Chem. C. 119, 25673–25683.

53 Lee, J. W., Seol, D. J., Cho, A. N., and Park, N. G. (2014). High-efficiency perovskite solar cells based on the black polymorph of $HC(NH_2)_2PbI_3$. Adv. Mater. 26, 4991–4998.

54 Eperon, G. E., Paternò, G. M., Sutton, R. J., Zampetti, A., Haghighirad, A. A., Cacialli, F., and Snaith, H. J. (2015). Inorganic caesium lead iodide perovskite solar cells. J. Mater. Chem. A. 3, 19688–19695.

55 Konstantakou, M., and Stergiopoulos, T. (2017). A critical review on tin halide perovskite solar cells. J. Mater. Chem. A. 5, 11518–11549.

56 Sutton, R. J., Eperon, G. E., Miranda, L., Parrott, E. S., Kamino, B. A., Patel, J. B., Hörantner, M. T., Johnston, M. B., Haghighirad, A. A., Moore, D. T., et al. (2016). Bandgap-tunable cesium lead halide perovskites with high thermal stability for efficient solar cells. Adv. Energy Mater. 6, 1502458.

57 Sabba, D., Mulmudi, H. K., Prabhakar, R. R., Krishnamoorthy, T., Baikie, T., Boix, P. P., Mhaisalkar, S., and Mathews, N. (2015). Impact of anionic Br- substitution on open circuit voltage in lead free perovskite ($CsSnI_{3-x}Br_x$) solar cells. J. Phys. Chem. C. 119, 1763–1767.

58 Jeon, N. J., Noh, J. H., Yang, W. S., Kim, Y. C., Ryu, S., Seo, J., and Seok, S. I. (2015). Compositional engineering of perovskite materials for high-performance solar cells. Nature. 517, 476–480.

59 Lee, J. W., Kim, D. H., Kim, H. S., Seo, S. W., Cho, S. M., and Park, N. G. (2015). Formamidinium and cesium hybridization for photo- and moisture-stable perovskite solar cell. Adv. Energy Mater. 5, 1501310

60 Mc Meekin, D. P., Sadoughi, G., Rehman, W., Eperon, G. E., Saliba, M., Horantner, M. T., Haghighirad, A., Sakai, N., Korte, L., Rech, B., et al. (2016). A mixed-cation lead mixed-halide perovskite absorber for tandem solar cells. Science 351, 151–155.

61 Saliba, M., Matsui, T., Seo, J.-Y., Domanski, K., Correa-Baena, J-P., Nazeeruddin, M. K., Zakeeruddin, S. M., Tress, W., Abate, A., Hagfeldt, A., et al. (2016). Cesium-containing triple cation perovskite solar cells: improved stability, reproducibility and high efficiency. Energy Environ. Sci. 9, 1989–1997.

62 Saliba, M., Matsui, T., Domanski, K., Seo, J.-Y., Ummadisingu, A., Zakeeruddin, S. M., Correa-Baena, J.-P., Tress, W. R., Abate, A., Hagfeldt, A., et al. (2016). Incorporation of rubidium cations into perovskite solar cells improves photovoltaic performance. Science 354, 206–209.

63 Park, Y. H., Jeong, I., Bae, S., Son, H. J., Lee, P., Lee, J., Lee, C.-H., and Ko, M. J. (2017). Inorganic rubidium cation as an enhancer for photovoltaic performance and moisture stability of $HC(NH_2)_2PbI_3$ perovskite solar cells. Adv. Funct. Mater. 27, 1605988.

64 Wu, C.-G., Chiang, C.-H., Tseng, Z.-L., Mohammad, K. N., Hagfeldt, A., and Grätzel, M. (2015). High efficiency stable inverted perovskite solar cells without current hysteresis. Energy Environ. Sci. 8, 2725–2733.

65 Wu, C.-G., Chiang, C.-H., and Chang, S. H. (2016). A perovskite cell with a record-high-V_{oc} of 1.61 V based on solvent annealed $CH_3NH_3PbBr_3$ /ICBA active layer. Nanoscale 8, 4077–4085.

66 Zha, B., Abdi-Jalebi, M., Tabachnyk, M., Glass, H., Kamboj, V. S., Nie, W., Pearson, A. J., Puttisong, Y., Gödel, K. C., Beere, H. E., et al. (2017). High open-circuit voltages in tin-rich low-bandgap perovskite-based planar heterojunction photovoltaics. Adv. Mater. 29, 1604744.

67 Zhao, D., Yu, Y., Wang, C., Liao, W., Shrestha, N., Grice, C. R., Cimaroli, A. J., Guan, L., Ellingson, R. J., Zhu, K., et al. (2017). Low-bandgap mixed tin–lead iodide perovskite absorbers with long carrier lifetimes for all-perovskite tandem solar cells. Nat. Energy 2, 17018.

68 Correa-Baena, J. P., Anaya, M., Lozano, G., Tress, W., Domanski, K., Saliba, M., Matsui, T., Jacobsson, T. J., Calvo, M. E., Abate, A., et al. (2016). Unbroken perovskite: interplay of morphology, electro-optical properties, and ionic movement. Adv. Mater. 28, 5031–5037.

69 Green, M. A. (2012). Radiative efficiency of state-of-the-art photovoltaic cells. Prog. Photovolt. Res. Appl. 20, 472–476.

70 Moriarty, T., and Emery, K. (2000). Procedures at NREL for evaluating multijunction concentrator cells. NCPV Program Review Meeting 71-72.

71 Chang, N. L., Ho-Bailie, A. W. Y., Basore, P.A.; Young, T. L., Evans, R., Egan, J. (2017). A manufacturing cost estimation method with uncertainty analysis and its application to perovskite on glass photovoltaic modules. Prog. Photovolt: Res. Appl. 25, 390-405.

72 Yoshikawa, K., Kawasaki, H., Yoshida, W., Irie, T., Konishi, K., Nakano, K., Uto, T., Adachi, D., Kanematsu, M., Uzu, H., et al. (2017). Silicon heterojunction solar cell with interdigitated back contacts for a photoconversion efficiency over 26%. Nat. Energy 2, 17032.

73 Mailoa, J. P., Bailie, C. D., Johlin, E. C., Hoke, E. T., Akey, A. J., Nguyen, W. H., McGehee, M. D., and Buonassisi, T. (2015). A 2-terminal perovskite/silicon multijunction solar cell enabled by a silicon tunnel junction. Appl. Phys. Lett. 106, 121105.

74 Albrecht, S., Saliba, M., Correa-Baena, J. P., Lang, F., Kegelmann, L., Mews, M., Steier, L., Abate, A., Rappich, J., Korte, L., et al. (2016). Monolithic perovskite/silicon-heterojunction tandem solar cells processed at low temperature. Energy Environ. Sci. 9, 81–88.

75 Werner, J., Weng, C. H., Walter, A., Fesquet, L., Seif, J. P., De Wolf, S., Niesen, B., and Ballif, C. (2016). Efficient monolithic perovskite/silicon tandem solar cell with cell area >1 cm^2. J. Phys. Chem. Lett. 7, 161–166.

76 Werner, J., Barraud, L., Walter, A., Bräuninger, M., Sahli, F., Sacchetto, D., Tétreault, N., Paviet-Salomon, B., Moon, S.-J., Allebé, C., et al. (2016). Efficient near-infrared-transparent perovskite solar cells enabling direct comparison of 4-terminal and monolithic perovskite/silicon tandem cells. ACS Energy Lett. 1, 474–480.

77 Bush, K. A., Palmstrom, A. F., Yu, Z. J., Boccard, M., Cheacharoen, R., Mailoa, J. P., McMeekin, D. P., Hoye, R. L. Z., Bailie, C. D., Leijtens, T., et al. (2017). 23.6%-Efficient monolithic perovskite/silicon tandem solar cells with improved stability. Nat. Energy. 2, 17009.

78 Filipič, M., Löper, P., Niesen, B., De Wolf, S. J. K., and Ballif. C. (2015). $CH_3NH_3PbI_3$ perovskite / silicon tandem solar cells: characterization based optical simulations. Opt. Express. 23, 263–278.

79 Santbergen, R., Mishima, R., Meguro, T., Hino, M., Uzu, H., Blanker, J., Yamamoto, K., and Zeman, M. (2016). Minimizing optical losses in monolithic perovskite/c-Si tandem solar cells with a flat top cell. Opt. Express. 24, A1288.

80 Shi, D., Zeng, Y., and Shen, W. (2015). Perovskite/c-Si tandem solar cell with inverted nanopyramids: realizing high efficiency by controllable light trapping. Sci. Rep. 5, 16504.

81 Albrecht, S., Saliba, M., Correa-Baena, J.-P., Jäger, K., Korte, L., Hagfeldt, A., Grätzel, M., and Rech, B. (2016). Towards optical optimization of planar monolithic perovskite/silicon-heterojunction tandem solar cells. J. Opt. 18, 64012.

82 Jiang, Y., Almansouri, I., Huang, S., Young, T., Li, Y., Peng, Y., Hou, Q., Spiccia, L., Bach, U., Cheng, Y-B., et al. (2016). Optical analysis of perovskite/silicon tandem solar cells. J. Mater. Chem. C. 4, 5679–5689.

83 Foster, S., and John, S. (2016). Light-trapping design for thin-film silicon-perovskite tandem solar cells. J. Appl. Phys. 120, 103103.

84 Liu, P., Liu, X., Lyu, L., Xie, H., Zhang, H., Niu, D., Huang, H., Bi, C., Xiao, Z., Huang, J., et al. (2015). Interfacial electronic structure at the $CH_3NH_3PbI_3/MoO_x$ interface. Appl. Phys. Lett. 106, 193903.

85 Bailie, C. D., Christoforo, M. G., Mailoa, J. P., Bowring, A. R., Unger, E. L., Nguyen, W. H., Burschka, J., Pellet, N., Lee, J. Z., Grätzel, M., et al. (2015). Semi-transparent perovskite solar cells for tandems with silicon and CIGS. Energy Environ. Sci. 8, 956–963.

86 Löper, P., Moon, S.-J., Martín de Nicolas, S., Niesen, B., Ledinsky, M., Nicolay, S., Bailat, J., Yum, J.-H., De Wolf, S., and Ballif, C. (2015). Organic–inorganic halide perovskite/crystalline silicon four-terminal tandem solar cells. Phys. Chem. Chem. Phys. 17, 1619–1629.

87 Duong, T., Lal, N., Grant, D., Jacobs, D., Zheng, P., Rahman, S., Shen, H., Stocks, M., Blakers, A., Weber, K., et al. (2016). semitransparent perovskite solar cell with sputtered front and rear electrodes for a four-terminal tandem. IEEE J. Photovoltaics. 6, 679–687.

88 Werner, J., Dubuis, G., Walter, A., Löper, P., Moon, S. J., Nicolay, S., Morales-Masis, M., De Wolf, S., Niesen, B., and Ballif, C. (2015). Sputtered rear electrode with broadband transparency for perovskite solar cells. Sol. Energy Mater. Sol. Cells. 141, 407–413.

89 Werner, J., Moon, S.-J., Löper, P., Walter, A., Filipič, M., Weng C. H., Löfgren, L., Bailat, J., Topič, M., Morales-Masis, M., et al. (2015). Towards ultra-high efficient photovoltaics with perovskite/crystalline silicon tandem devices. 31st Eur. PV Sol. Energy Conf. Exhib. 14–18.

90 Bush, K. A., Bailie, C. D., Chen, Y., Bowring, A. R., Wang, W., Ma, W., Leijtens, T., Moghadam, F and McGehee, M. D. (2016). Thermal and environmental stability of semi-transparent perovskite solar cells for tandems enabled by a solution-processed nanoparticle buffer layer and sputtered ITO Electrode. Adv. Mater. 28, 3937–3943.

91 Chen, B., Bai, Y., Yu, Z., Li, T., Zheng, X., Dong, Q., Shen, L., Boccard, M., Gruverman, A., Holman, Z., et al. (2016). Efficient semitransparent perovskite solar cells for 23.0%-efficiency perovskite/silicon four-terminal tandem cells. Adv. Energy Mater. 6, 16001128.

92 Duong, T., Wu, Y., Shen, H., Peng, J., Fu, X., Jacobs, D., Wang, E. C., Kho, T. C., Fong, K. C., Stocks, M., et al. (2017). Rubidium multication perovskite with optimized bandgap for perovskite-silicon tandem with over 26% efficiency. Adv. Energy Mater. 7, 1700228.

93 Uzu, H., Ichikawa, M., Hino, M., Nakano, K., Meguro, T., Hernández, J. L., Kim, H. S., Park, N. G., and Yamamoto, K. (2015). High efficiency solar cells combining a perovskite and a silicon heterojunction solar cells via an optical splitting system. Appl. Phys. Lett. 106, 3–7.

94 Sheng, R., Ho-Baillie, A. W. Y., Huang, S., Keevers, M., Hao, X., Jiang, L., Cheng, Y.-B., and Green, M. A. (2015). Four-terminal tandem solar cells using $CH_3NH_3PbBr_3$ by spectrum splitting. J. Phys. Chem. Lett. 6, 3931–3934.

95 Kinoshita, T., Nonomura, K., Jeon, J. N., Giordano, F., Abate, A., Uchida, S., Kubo, T., Seok, S. I., Nazeeruddin, M. K., Hagfeldt, A., et al. (2015). Spectral splitting photovoltaics using perovskite and wideband dye-sensitized solar cells. Nat. Commun. 6, 8834.

96 Todorov, T., Gershon, T., Gunawan, O., Lee, Y. S., Sturdevant, C., Chang, L. Y., and Guha, S. (2015). Monolithic perovskite-CIGS tandem solar cells via in situ band gap engineering. Adv. Energy Mater. 5, 1500799.

97 Lee, M., Park, S. J., Hwang, Y. J., Jun, Y., and Min, B. K. (2016). Tandem architecture of perovskite and $Cu(In,Ga)(S,Se)_2$ created by solution processes for solar cells. Adv. Opt. Mater. 4, 2102–2108.

98 Kranz, L., Abate, A., Feurer, T., Fu, F., Avancini, E., Löckinger, J., Reinhard, P., Zakeeruddin, S. M., Grätzel, M., Buecheler, S., et al. (2015). High-efficiency polycrystalline thin film tandem solar cells. J. Phys. Chem. Lett. 6, 2676–2681.

99 Yang, Y. M., Chen, Q., Hsieh, Y.-T., Song, T.-B., De Marco, N., Zhou, H., and Yang, Y. (2015). Multilayer transparent top electrode for solution processed perovskite/Cu(In,Ga)(Se,S)$_2$ four terminal tandem solar cells. ACS Nano 9, 7714–7721.

100 Fu, F., Feurer, T., Jäger, T., Avancini, E., Bissig, B., Yoon, S., Buecheler, S., and Tiwari, A. N. (2015). Low-temperature-processed efficient semi-transparent planar perovskite solar cells for bifacial and tandem applications. Nat. Commun. 6, 8932.

101 Fu, F., Feurer, T., Weiss, T. P., Pisoni, S., Avancini, E., Andres, C., Buecheler, S., and Tiwari, A. N. (2016). High-efficiency inverted semi-transparent planar perovskite solar cells in substrate configuration. Nat. Energy. 2, 16190.

102 Guchhait. A., Dewi, H. A., Leow, S. W., Wang, H., Han, G., Suhaimi, F. B., Mhaisalkar, S., Wong, L. H., and Mathews, N. (2017). Over 20% efficient CIGS–perovskite tandem solar cells. ACS Energy Lett. 2, 807–812.

103 Todorov, T., Gershon, T., Gunawan, O., Sturdevant, C., and Guha, S. (2014). Perovskite-kesterite monolithic tandem solar cells with high open-circuit voltage. Appl. Phys. Lett. 105, 173902.

104 Li, Y., Hu, H., Chen, B., Salim, T., Lam, Y. M., Yuan, N., and Ding, J. (2017). Solution-processed perovskite-kesterite reflective tandem solar cells. Sol. Energy. 155, 35–38.

105 Chen, C.-W., Hsiao, S.-Y., Chen, C.-Y., Kang, H.-W., Huang, Z.-Y., and Lin, H.-W. (2015). Optical properties of organometal halide perovskite thin films and general device structure design rules for perovskite single and tandem solar cells. J. Mater. Chem. A. 3, 9152–9159.

106 Heo, J. H., and Im, S. H. (2016). $CH_3NH_3PbBr_3$-$CH_3NH_3PbI_3$ perovskite-perovskite tandem solar cells with exceeding 2.2 V open circuit voltage. Adv. Mater. 28, 5121–5125.

107 Jiang, F., Liu, T., Luo, B., Tong, J., Qin, F., Xiong, S., Li, Z., and Zhou, Y. (2016). A two-terminal perovskite/perovskite tandem solar cell. J. Mater. Chem. A 4, 1208–1213.

108 Forgács, D., Gil-Escrig, L., Pérez-del-Rey, D., Momblona, C., Werner, J., Niesen, B., Ballif, C., Sessolo, M., and Bolink, H. J. (2017). Efficient monolithic perovskite/perovskite tandem solar cells. Adv. Energy. Mater. 7, 1602121.

109 Yang, Z., Rajagopal, A., Chueh, C. C., Jo, S. B., Liu, B., Zhao, T., and Jen, A. K. Y. (2016). Stable low-bandgap Pb-Sn binary perovskites for tandem solar cells. Adv. Mater. 28, 8990–8997.

110 Rajagopal, A., Yang, Z., Jo, S. B., Braly, I. L., Liang, P.-W., Hillhouse, H. W., and Jen, A. K.-Y. (2017). Highly efficient perovskite-perovskite tandem solar cells reaching 80% of the theoretical limit in photovoltage. Adv. Mater. 1702140.

111 Chen, C.-C., Bae, S.-H., Chang, W.-H., Hong, Z., Li, G., Chen, Q., Zhou, H., and Yang, Y. (2015). Perovskite/polymer monolithic hybrid tandem solar cells utilizing a low-temperature, full solution process. Mater. Horiz. 2, 203–211.

112 Liu, Y., Renna, L. A., Bag, M., Page, Z. A., Kim, P., Choi, J., Emrick, T., Venkataraman, D., and Russell, T. P. (2016). High efficiency tandem thin-perovskite/polymer solar cells with a graded recombination layer. ACS Appl. Mater. Interfaces. 8, 7070–7076.

113 Ren, Z., Ng, A., Shen, Q., Gokkaya, H. C., Wang, J., Yang, L., Yiu, W.-K., Bai, G., Djurišić, A. B., Leung, W. W., et al. (2014). Thermal assisted oxygen annealing for high efficiency planar $CH_3NH_3PbI_3$ perovskite solar cells. Sci. Rep. 4, 6752.

114 Yu, H., Liu, X., Xia, Y., Dong, Q., Zhang, K., Wang, Z., Zhou, Y., Song, B., and Li, Y. (2016). Room-temperature mixed-solvent-vapor annealing for high performance perovskite solar cells. J. Mater. Chem. A 4, 321–326.

115 Lin, Q., Armin, A., Nagiri, R. C. R., Burn, P. L., and Meredith, P. (2015). Electro-optics of perovskite solar cells. Nat. Photon. 9, 106–112.

116 Löper, P., Stuckelberger, M., Niesen, B., Werner, J., Filipi, M., Moon, S., Yum, J., Topi, M., De Wolf, S., and Ballif, C. (2015). Complex refractive index spectra of $CH_3NH_3PbI_3$ perovskite thin films determined by spectroscopic ellipsometry and spectrophotometry. J. Phys. Chem. Lett. 6, 66–71.

117 Carretero-Palacios, S., Jiménez-Solano, A., and Míguez, H. (2016). Plasmonic Nanoparticles as Light-Harvesting Enhancers in Perovskite Solar Cells: A User's Guide. ACS Energy Lett. 1, 323–331.

118 Khanarian, G., Joo, J., Liu, X. Q., Eastman, P., Werner, D., O'Connell, K., and Trefonas, P. (2013). The optical and electrical properties of silver nanowire mesh films. J. Appl. Phys. 114, 024302.

119 Jean, J., Wang ,A., and Bulovic, V. (2016). In situ vapor-deposited parylene substrates for ultra-thin, lightweight organic solar cells. Org. Electron. Physics Mater. Appl. 31, 120–126.

120 Jacobs, D. A., Catchpole, K. R., Beck, F. J., and White, T. P. (2016). A re-evaluation of transparent conductor requirements for thin-film solar cells. J. Mater. Chem. A. 4, 4490–4496.

121 Momblona, C., Gil-Escrig, L., Bandiello, E., Hutter, E. M., Sessolo, M., Lederer, K., Blochwitz-Nimoth, J., Bolink, H. J., Kojima, A., Teshima, K., et al. (2016). Efficient vacuum deposited p-i-n and n-i-p perovskite solar cells employing doped charge transport layers. Energy Environ. Sci. 9, 3456–3463.

122 Prosser, J. H., Brugarolas, T., Lee, S., Nolte, A. J., and Lee, D. (2012). Avoiding cracks in nanoparticle films. Nano Lett. 12, 5287–5291.

123 Bella, F., Griffini, G., Correa-Baena, J.-P., Saracco, G., Gratzel, M., Hagfeldt, A., Turri, S., and Gerbaldi, C. (2016). Improving efficiency and stability of perovskite solar cells with photocurable fluoropolymers. Science 354, 203–206.

124 Li, S.-G., Jiang, K.-J., Su, M.-J., Cui, X.-P., Huang, J.-H., Zhang, Q.-Q., Zhou, Z.-Q., Yanga, L.-M., and Song, Y.-L. (2015). Inkjet printing of $CH_3NH_3PbI_3$ on a mesoscopic TiO_2 film for highly efficient perovskite solar cells. J. Mater. Chem. A 3, 9092-9097.

125 Ciro, J., Mejía-Escobar, M. A., and Jaramillo, F. (2017). Slot-die processing of flexible perovskite solar cells in ambient conditions. Sol. Ener. 150, 570-576.

126 Hwang, K., Jung, Y.-S., Heo, Y.-J., Scholes, F. H., Watkins, S. E., Subbiah, J., Jones, D. J., Kim, D.-Y., and Vak, D. (2015). Toward large scale roll-to-roll production of fully printed perovskite solar cells. Adv. Mater. 27, 1241-1247.

127 Shao, Y., Fang, Y., Li, T., Wang, Q., Dong, Q., Deng, Y., Yuan, Y., Wei, H., Wang, M., Gruverman, A., et al. (2016). Grain boundary dominated ion migration in polycrystalline organic–inorganic halide perovskite films. Energy Environ. Sci. 2016, 9, 1752.

128 Gholipour, S., Ali, A. M., Correa-Baena, J.-P., Turren-Cruz, S. H., Tajabadi, F., Tress, W., Taghavinia, N., Grätzel, M., Abate, A., De Angelis, F., et al. (2017). Globularity-selected large molecules for a new generation of multication perovskites. Adv. Mater. DOI: 10.1002/adma.201702005.

129 Zeitouny, J., Katz, E. A., Dollet, A., and Vossier, A. (2017). Band gap engineering of multi-junction solar cells: effects of series resistances and solar concentration. Sci. Rep. 7, 1766.

130 Zhang, W., Anaya, M., Lozano, G., Calvo, M. E., Johnston, M. B., Míguez, H., and Snaith, H. J. (2015). Highly efficient perovskite solar cells with tunable structural color. Nano Lett. 15, 1698–1702.

131 Ramírez Quiroz, C. O., Bronnbauer, C., Levchuk, I., Hou, Y., Brabec, C. J., and Forberich, K. (2016). Coloring semitransparent perovskite solar cells via dielectric mirrors. ACS Nano 10, 5104–5112.

132 Anaya, M., Zhang, W., Hames, B. C., Li, Y., Fabregat-Santiago, F., Calvo, M. E., Snaith, H. J., Míguez, H., and Mora-Seró, I. (2017). Electron injection and scaffold effects in perovskite solar cells. J. Mater. Chem. C 5, 634–655.

133 Lin, A., Fu, S. M., Chen, B.-R., Yan, S.-L., Zhong, Y. K., Kao, M.-H., Shen, C.-H., Shieh, J.-M., and Tseng, T. Y. (2016). The external light trapping for perovskite solar cells using nanoimprinted polymer metamaterial patterns. Photovol. Spec. Conf. (PVSC) IEEE. DOI: 10.1109/PVSC.2016.7749605.

134 Mao, J., Sha, W. E. I., Zhang, H., Ren, X., Zhuang, J., Roy, V. A. L., Wong, K. S., and Choy, W. C. H. (2017). Novel direct nanopatterning approach to fabricate periodically nanostructured perovskite for optoelectronic applications. Adv. Funct. Mater. 27, 1606525.

135 Saliba, M., Wood, S. M., Patel, J. B., Nayak, P. K., Huang, J., Alexander-Webber, J. A., Wenger, B., Stranks, S. D., Hörantner, M. T., Wang, J. T.-W., et al. (2016). Structured organic–inorganic perovskite toward a distributed feedback laser. Adv. Mater. 28, 923–929.

136 Yin, J., Qu, H., Cao, J., Tai, H., Li, J., and Zheng, N. (2016). Light absorption enhancement by embedding submicron scattering TiO_2 nanoparticles in perovskite solar cells. RSC Adv. 6, 24596–24602.